Electronic supplementary information

for

Photophysical properties and electron transfer photochemical reactivity of substituted phthalimides

Leo Mandić,[a,b] Iva Džeba,[b] Dijana Jadreško,[c] Branka Mihaljević,[b] László Biczók,[d] Nikola Basarić[a]*

[a] Department of Organic Chemistry and Biochemistry, Ruđer Bošković Institute, Bijenička cesta 54, 10000 Zagreb, Croatia. Fax: +385 1 4680 195; Tel: +385 12 4561 141; E-mail: nbasaric@irb.hr
[b] Department of Material Chemistry, Ruđer Bošković Institute, Bijenička cesta 54, 10000 Zagreb, Croatia.
[c] Laboratory for Physical Chemistry of Traces, Division for Marine and Environmental Research, Ruđer Bošković Institute, Bijenička cesta 54, 10000 Zagreb, Croatia.
[d] Institute of Materials and Environmental Chemistry, Research Centre for Natural Sciences, Hungarian Academy of Sciences, 1519 Budapest, P.O. Box 286, Hungary

Content:

1. Photochemical experiments

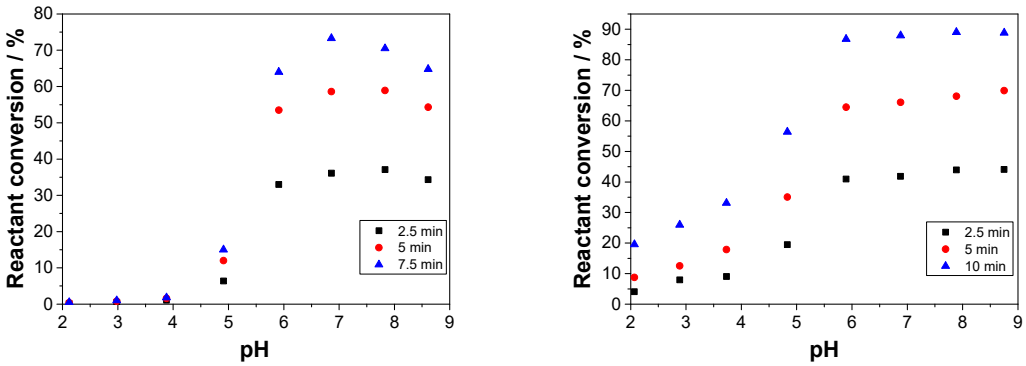

Fig S1. Photodecarboxylation efficiency of **2** at different buffer pH values (left: CH_3CN-H_2O (1:1 - v/v), right: acetone-H_2O (1:1 - v/v); *c* (**2**) = 10^{-3} mol dm^{-3}, *c* (phosphate) = 0.05 mol dm^{-3}).

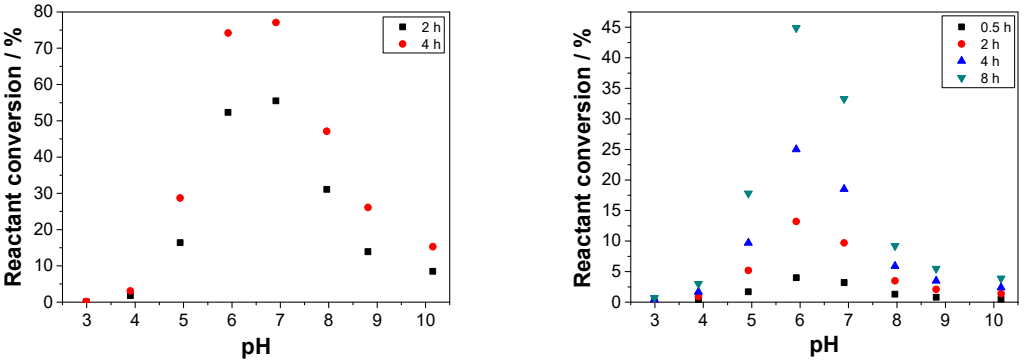

Fig S2. Photodecarboxylation efficiency of **4** at different buffer pH values (left: CH_3CN-H_2O (1:1 - v/v), right: acetone-H_2O (1:1 - v/v); *c* (**4**) = 10^{-3} mol dm^{-3}, *c* (phosphate) = 0.05 mol dm^{-3}).

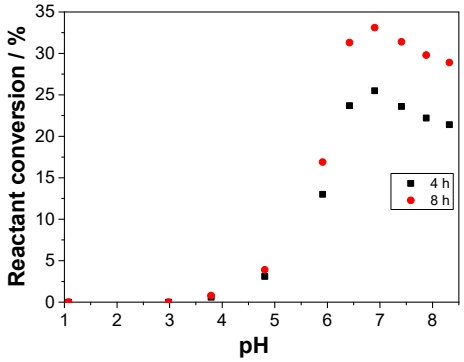

Fig S3. Photodecarboxylation efficiency of **6** at different buffer pH values (CH_3CN-H_2O (1:1 - v/v); *c* (**6**) = 10^{-3} mol dm^{-3}, *c* (phosphate) = 0.05 mol dm^{-3}).

Photochemical reaction quantum yield was caculated according to:

$$\Phi = \Phi_R \frac{x}{x_R} \frac{A}{A_R} \frac{\varepsilon_R}{\varepsilon} \frac{1-10^{-A_R}}{1-10^{-A}} \quad \text{(S1)}$$

Φ and Φ_R – photodecarboxylation quantum yield of compound and the actinometer;
x and x_R – conversion of compound and the actinometer;
A and A_R – absorbance of compound and the actinometer at the irradiation wavelength;
ε and ε_R – molar absorption coefficient of compound and the actinometer at the irradiation wavelength.

2. Cyclic voltammetry

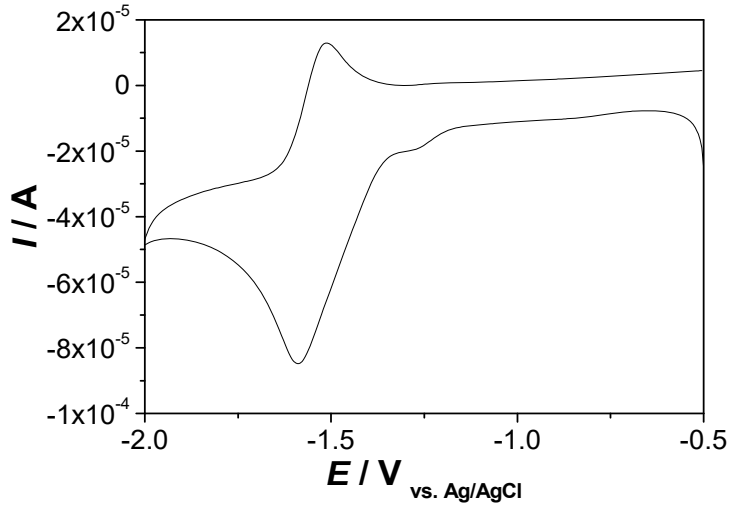

Fig S4. Cyclic voltammogram of **1** (c = 10^{-3} mol dm^{-3}) in N_2-purged CH_3CN in the presence of NBu_4PF_6 (c = 0.1 mol dm^{-3}).

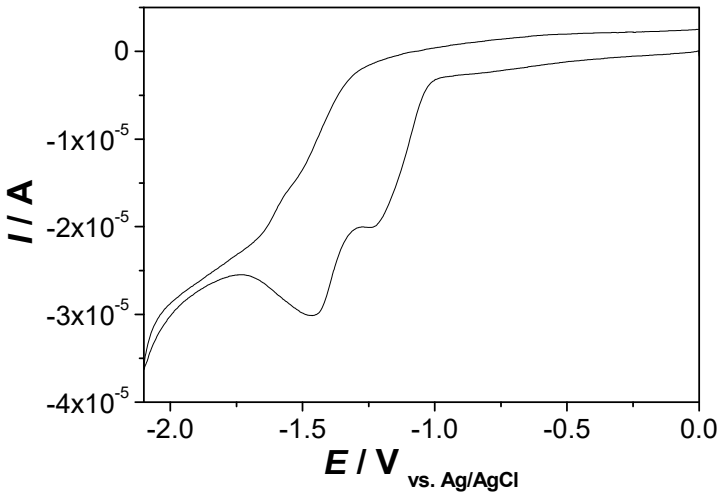

Fig S5. Cyclic voltammogram of **2** (c = 10^{-3} mol dm^{-3}) in N_2-purged CH_3CN in the presence of NBu_4PF_6 (c = 0.1 mol dm^{-3}).

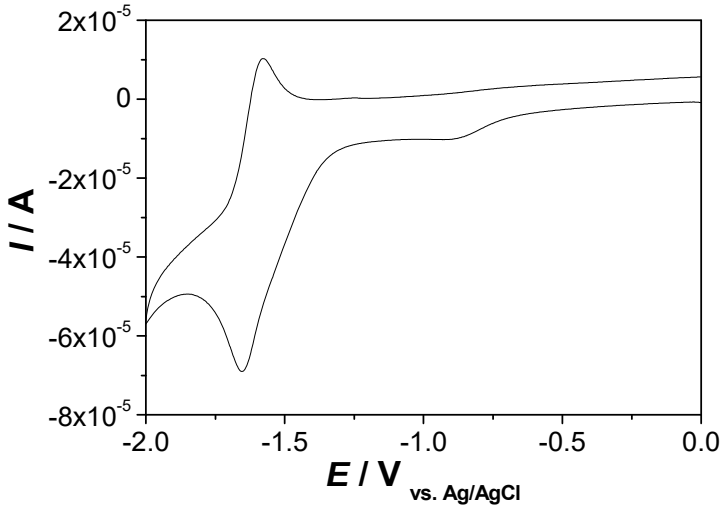

Fig S6. Cyclic voltammogram of **3** (c = 10^{-3} mol dm^{-3}) in N_2-purged CH_3CN in the presence of NBu_4PF_6 (c = 0.1 mol dm^{-3}).

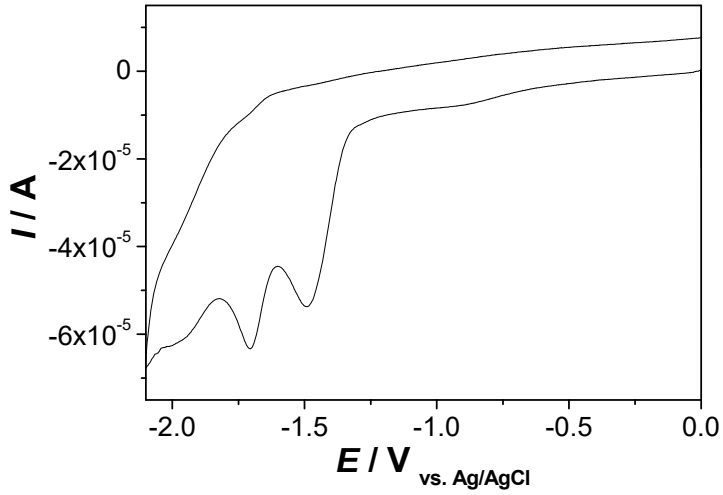

Fig S7. Cyclic voltammogram of **4** (c = 10^{-3} mol dm^{-3}) in N_2-purged CH_3CN in the presence of NBu_4PF_6 (c = 0.1 mol dm^{-3}).

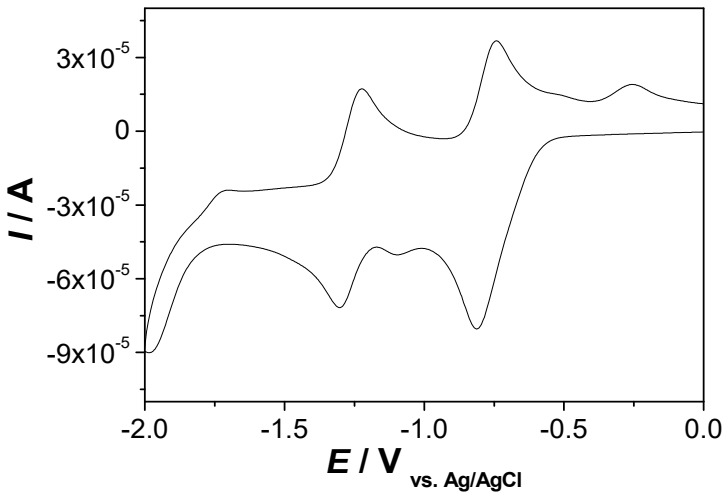

Fig S8. Cyclic voltammogram of **5** (c = 10^{-3} mol dm^{-3}) in N_2-purged CH_3CN in the presence of NBu_4PF_6 (c = 0.1 mol dm^{-3}).

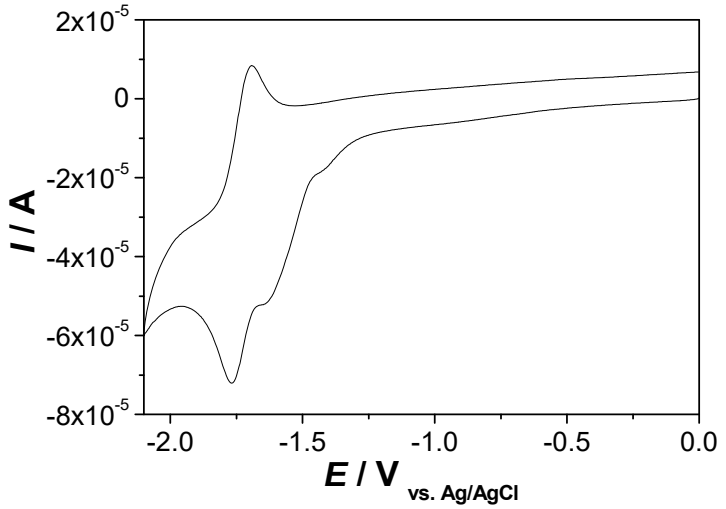

Fig S9. Cyclic voltammogram of **6** (c = 10^{-3} mol dm^{-3}) in N_2-purged CH_3CN in the presence of NBu_4PF_6 (c = 0.1 mol dm^{-3}).

The work for the separation of charges, needed for the estimation of the Gibbs energy for PET was estimated from:

$$w(\mathrm{D}^{+\cdot}\mathrm{A}^{-\cdot})/\mathrm{Jmol}^{-1} = N_\mathrm{A} z(\mathrm{D}^{+\cdot}) z(\mathrm{A}^{-\cdot}) e^2/(4\pi\epsilon_0\epsilon_\mathrm{r} a) \qquad \text{(S2)}$$

Where:

N_A Avogadro number, 6.022×10^{23} mol^{-1}

a 5 Å, distance between the donor (carboxylate) and acceptor (phthalimide), computed by CAM-B3LYP/cc-pVTZ

z charge (+1 or -1)

e elementary charge, 1.602×10^{-19} C

$e^2/(4\pi\ \varepsilon_0) = 2.307 \times 10^{-28}$ J m

ε_0 permittivity of vacuum (8.854×10^{-12} C^2 J^{-1} m^{-1})

ε_r relative statistic permittivity (for H_2O ε_r 80.16)

3. UV-Vis and fluorescence spectroscopy

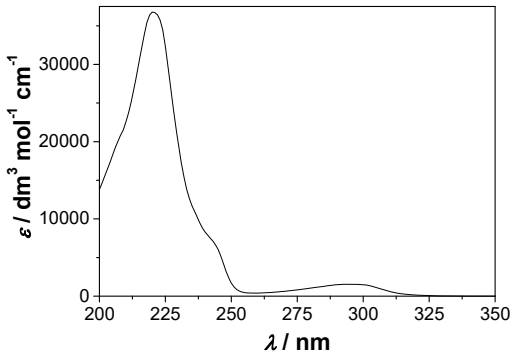

Fig S10. Absorption spectrum of **1** in CH_3CN.

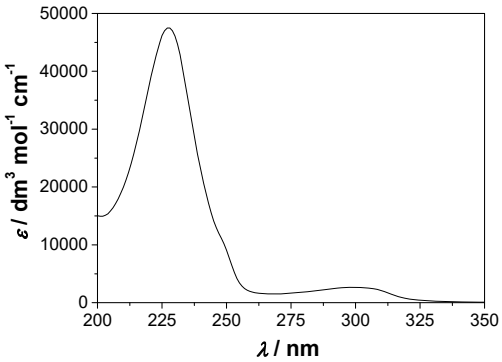

Fig S11. Absorption spectrum of **2** in CH_3CN.

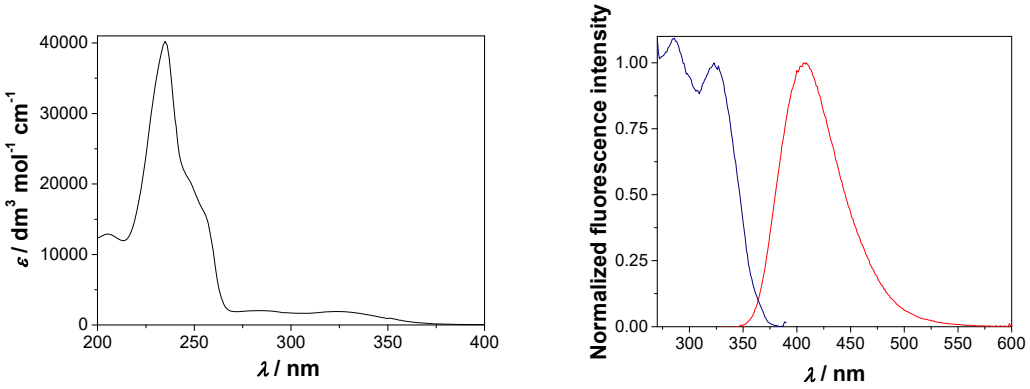

Fig S12. Absorption spectrum (left) and normalized emission (red line, λ_{exc} = 310 nm) and excitation spectra of **3** (blue line, λ_{em} = 400 nm) in CH_3CN at 25 °C (right).

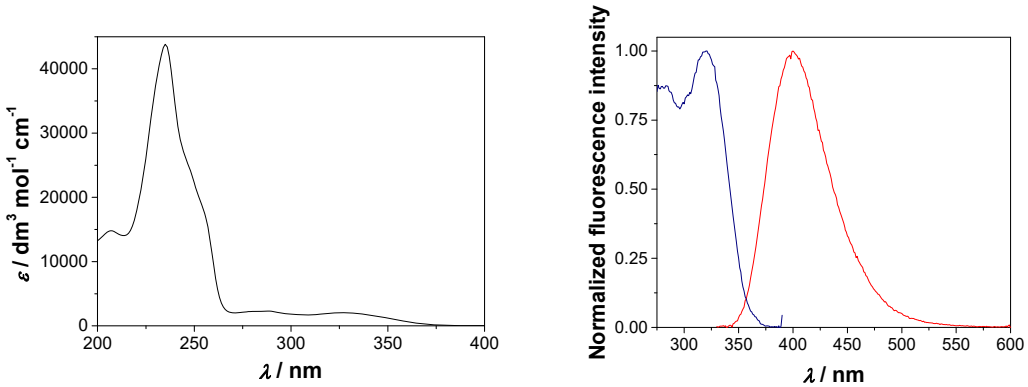

Fig S13. Absorption spectrum (left) and normalized emission (red line, λ_{exc} = 310 nm) and excitation spectra of **4** (blue line, λ_{em} = 400 nm) in CH_3CN at 25 °C (right).

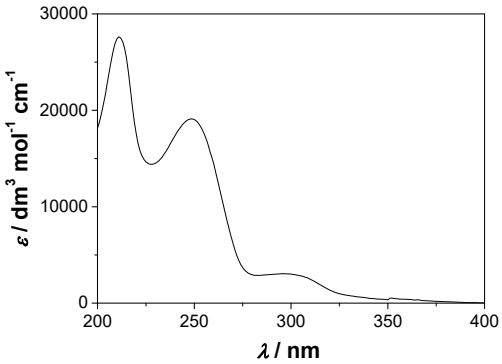

Fig S14. Absorption spectrum of **5** in CH_3CN.

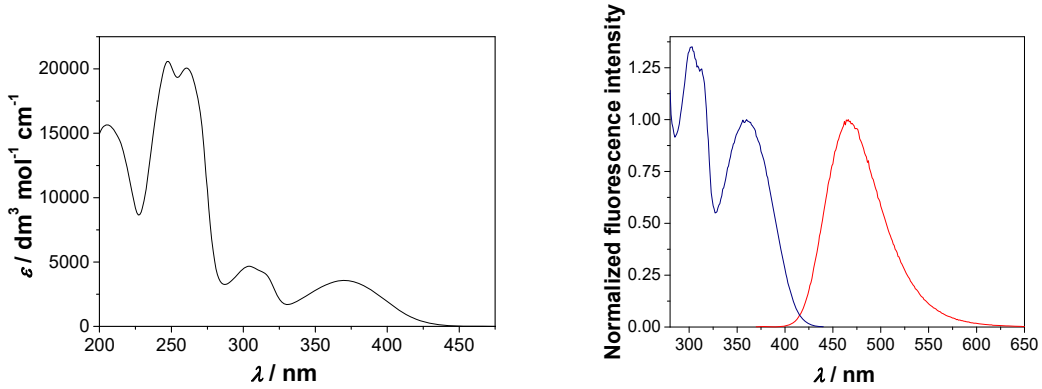

Fig S15. Absorption spectrum (left) and normalized emission (red line, λ_{exc} = 360 nm) and excitation spectrum of **6** (blue line, λ_{em} = 470 nm) in CH_3CN at 25 °C (right).

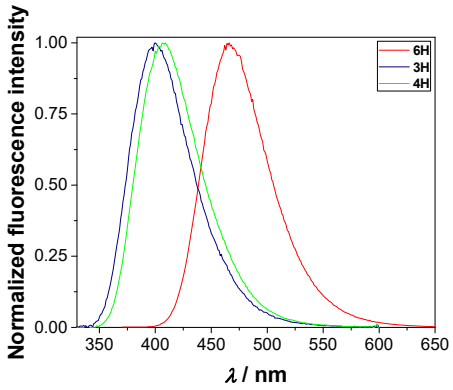

Fig S16. Normalized emission spectra of **6H** (λ_{exc} = 360 nm), **3H** (λ_{exc} = 310 nm) and **4H** (λ_{exc} = 310 nm) in CH_3CN at 25 °C.

Fluorescence quantum yield was calculated according to:

$$\Phi = \Phi_R \left(\frac{n}{n_R}\right)^2 \frac{I}{I_R} \frac{1-10^{-A_R}}{1-10^{-A}} \qquad \text{(S3)}$$

Φ and Φ_R – fluorescence quantum yield of compound and the reference;
n and n_R – refractive index of the solvent in which compound or the reference was dissolved;
A and A_R – absorbance of compound and reference at the excitation wavelength;
I and I_R – area under emission curve of compound and the reference.

Fluorescence decays were obtained with time-correlated single-photon counting method. A Picoquant diode laser (pulse duration ~70 ps, wavelength 368 nm) served as excitation light source. The fluorescence signals were monitored with a Hamamatsu R3809U-51 microchannel plate photomultiplier, which was connected to a Picoquant Timeharp 100 electronics having 36 ps/channel time resolution. The histograms were analyzed by a nonlinear least-squares deconvolution method using Picoquant FluoFit software. The quality of the fit was judged by the reduced χ^2 being close to unity and the random distribution of the weighted residuals. Fluorescence decays were fit to a sum of exponentials using the following expression:

$$F(t) = \alpha_1 \exp\left(-\frac{t}{\tau_1}\right) + \alpha_2 \exp\left(-\frac{t}{\tau_2}\right) + \alpha_3 \exp\left(-\frac{t}{\tau_3}\right) + \ldots \qquad \text{(S4)}$$

Table S1. Lifetimes and pre-exponential factors obtained from the analysis of fluorescence decays for **3**, **4** and **6**.

Molecule/solvent	τ / ns [a]	Pre-exponential factors [b]			
		390 nm	410 nm	440 nm	470 nm
3/CH_3CN	1.68 ± 0.01	1.00	0.99	0.95	0.85
	16.0 ± 0.4		0.01	0.05	0.15
3/CH_3CN-H_2O	4.6 ± 0.2	0.20	0.14	0.10	0.09
pH 4.5	24.7 ± 1.0	0.80	0.86	0.90	0.91
3/CH_3CN-H_2O	0.46 ± 0.01	0.88	0.93	0.97	0.99
pH 8.3	23.7 ± 1.0	0.12	0.07	0.03	0.01
4/CH_3CN	2.33 ± 0.08	0.97	0.95	0.92	0.90
	14.7 ± 0.3	0.03	0.05	0.08	0.10
		450 nm	475 nm	500 nm	620 nm
4/CH_3CN-H_2O	≤ 0.1	0.99	0.93	0.90	0.26
pH 4.5	2.4 ± 0.3	0.003	0.068	0.08	0.74
	22.0 ± 0.8	0.007	0.003	0	0
4/CH_3CN-H_2O	≤ 0.1	0.99	0.92	0.28	0
pH 6.4	2.20 ± 0.06	0.008	0.08	0.72	1.00
4/CH_3CN-H_2O	1.88 ± 0.01				
pH 8.3					
6/CH_3CN	17.2 ± 0.2				
		460 nm	490 nm	520 nm	550 nm
6/CH_3CN-H_2O	0.4 ± 0.1	0.48	0.21	0	0
pH 4.5	7.32 ± 0.05	0.52	0.79	1.00	1.0
6/CH_3CN-H_2O	0.4 ± 0.1	0.43	0	0	0
pH 8.3	5.84 ± 0.07	0.57	1.00	1.00	1.00

[a] The quoted errors correspond to the maximum absolute deviations. [b] Estimated errors on pre-exponential factors range from 5% for the main decay components up to 30% for the minor decay components.

4. Determination of pK_a values

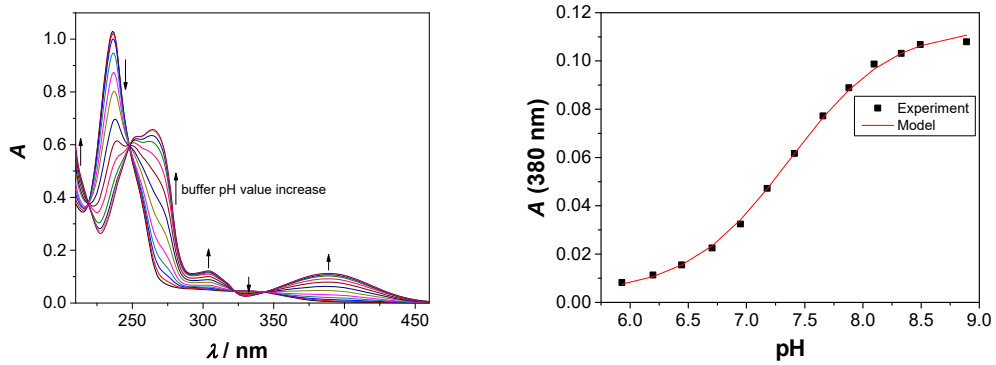

Fig S17. Absorption spectra of **4** (c = 2.72 × 10^{-5} mol dm^{-3}) in CH_3CN-H_2O (1:9 - v/v) in the presence of phosphate buffer (c = 0.05 mol dm^{-3}) at different buffer pH values (left) and dependence of the absorbance at 380 nm on pH (right); black dots are the measured values and the red line corresponds to the calculated values by nonlinear regression analysis with Specfit software. The measurements were conducted at 25 °C.

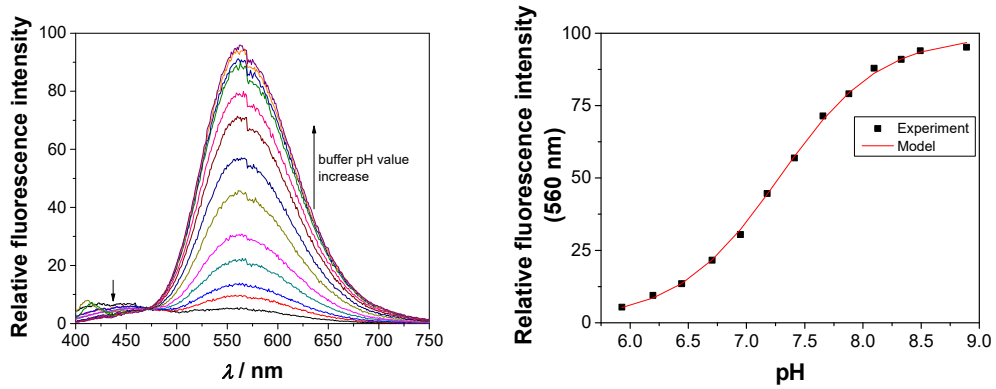

Fig S18. Emission spectra of **4H** (λ_{exc} = 380 nm, c = 3.30 × 10^{-5} mol dm^{-3}) in CH_3CN-H_2O (1:9 - v/v) in the presence of phosphate buffer (c = 0.05 mol dm^{-3}) at different buffer pH values (left) and dependence of the fluorescence intensity at 560 nm on pH (right); black dots are the measured values and the red line corresponds to the calculated values by nonlinear regression analysis with Specfit software. The measurements were conducted at 25 °C.

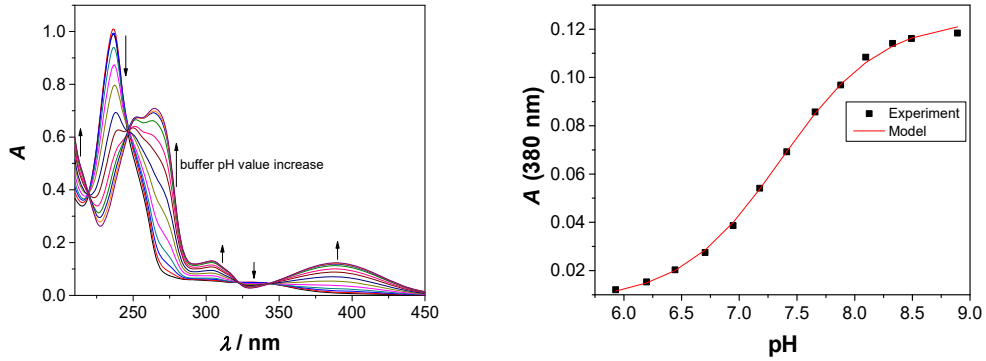

Fig S19. Absorption spectra of **4H** (c = 3.30 × 10^{-5} mol dm^{-3}) in CH_3CN-H_2O (1:9 - v/v) in the presence of phosphate buffer (c = 0.05 mol dm^{-3}) at different buffer pH values (left) and dependence of the absorbance at 380 nm on pH (right); black dots are the measured values and the red line corresponds to the calculated values by nonlinear regression analysis with Specfit software. The measurements were conducted at 25 °C.

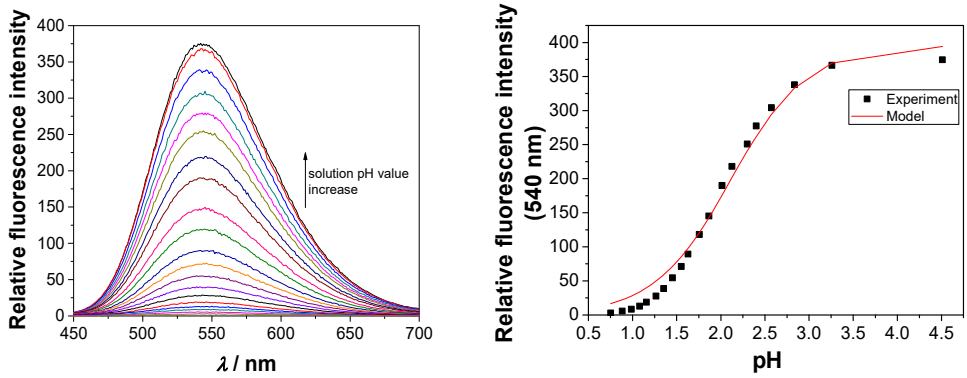

Fig S20. Emission spectra of **6** (λ_{exc} = 370 nm, c = 1.75 × 10^{-5} mol dm^{-3}) in CH_3CN-H_2O (1:9 - v/v) in the presence of KCl (c = 2 mol dm^{-3}) at different solution pH values (left) and dependence of the fluorescence intensity at 540 nm on pH (right); black dots are the measured values and the red line corresponds to the calculated values by nonlinear regression analysis with Specfit software. The measurements were conducted at 25 °C.

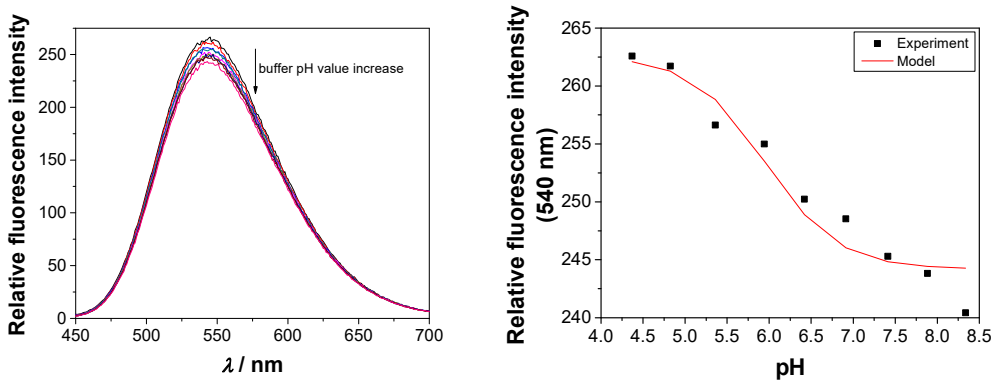

Fig S21. Emission spectra of **6** (λ_{exc} = 370 nm, c = 1.76 × 10^{-5} mol dm^{-3}) in CH_3CN-H_2O (1:9 - v/v) in the presence of phosphate buffer (c = 0.05 mol dm^{-3}) at different buffer pH values (left) and dependence of the fluorescence intensity at 540 nm on pH (right); black dots are the measured values and the red line corresponds to the calculated values by nonlinear regression analysis with Specfit software. The measurements were conducted at 25 °C.

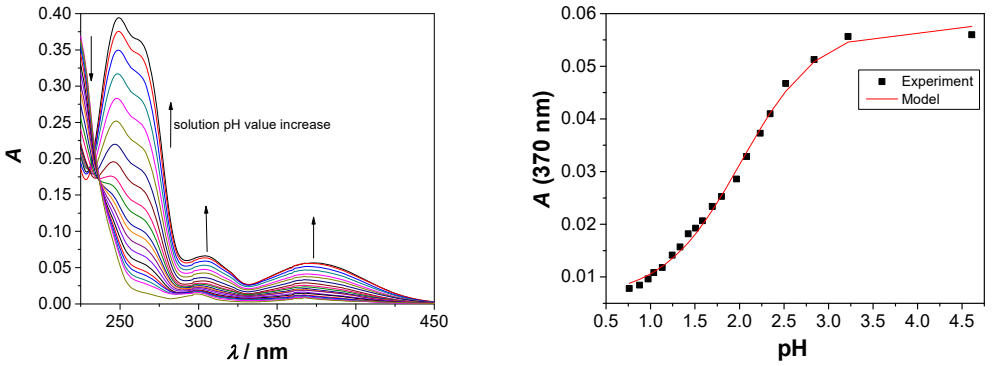

Fig S22. Absorption spectra of **6H** (c = 1.84 × 10^{-5} mol dm^{-3}) in CH_3CN-H_2O (1:9 - v/v) in the presence of KCl (c = 2 mol dm^{-3}) at different solution pH values (left) and dependence of the absorbance at 370 nm on pH (right); black dots are the measured values and the red line corresponds to the calculated values by nonlinear regression analysis with Specfit software. The measurements were conducted at 25 °C.

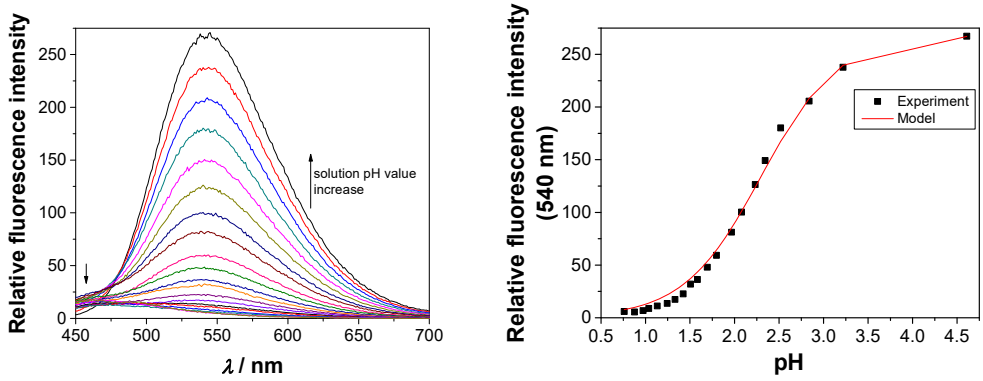

Fig S23. Emission spectra of **6H** (λ_{exc} = 370 nm, c = 1.84 × 10^{-5} mol dm^{-3}) in CH_3CN-H_2O (1:9 - v/v) in the presence of KCl (c = 2 mol dm^{-3}) at different solution pH values (left) and dependence of the fluorescence intensity at 540 nm on pH (right); black dots are the measured values and the red line corresponds to the calculated values by nonlinear regression analysis with Specfit software. The measurements were conducted at 25 °C.

5. Laser Flash Photolysis

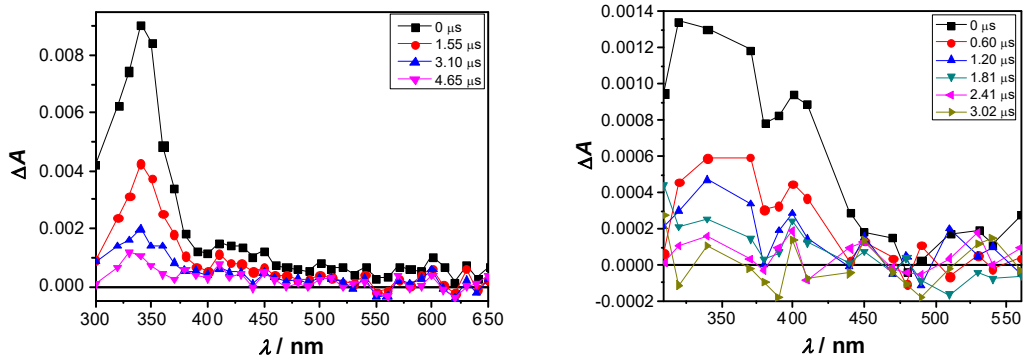

Fig S24. Transient absorption spectra of **1** (c = 4.41 × 10^{-4} mol dm^{-3}) in N_2-purged CH_3CN-H_2O (1:1 - v/v) in the presence of phosphate buffer (c = 0.05 mol dm^{-3}) at pH 4 (left) and pH 7 (right). E_{laser} = 20 mJ.

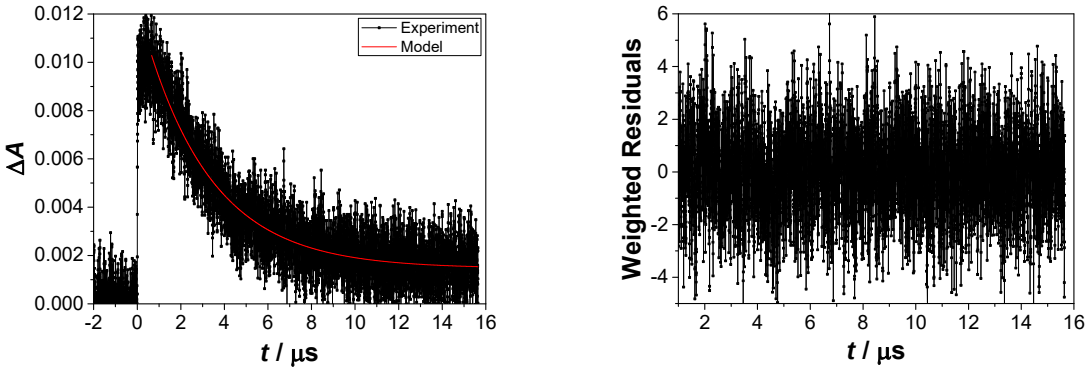

Fig S25. Decay of transient absorbance at 330 nm for N_2-purged CH_3CN-H_2O (1:1 - v/v) solution of **1** in the presence of phosphate buffer (c = 0.05 mol dm^{-3}) at pH 4 (left), and the corresponding weighted residuals (right). E_{laser} = 16 mJ.

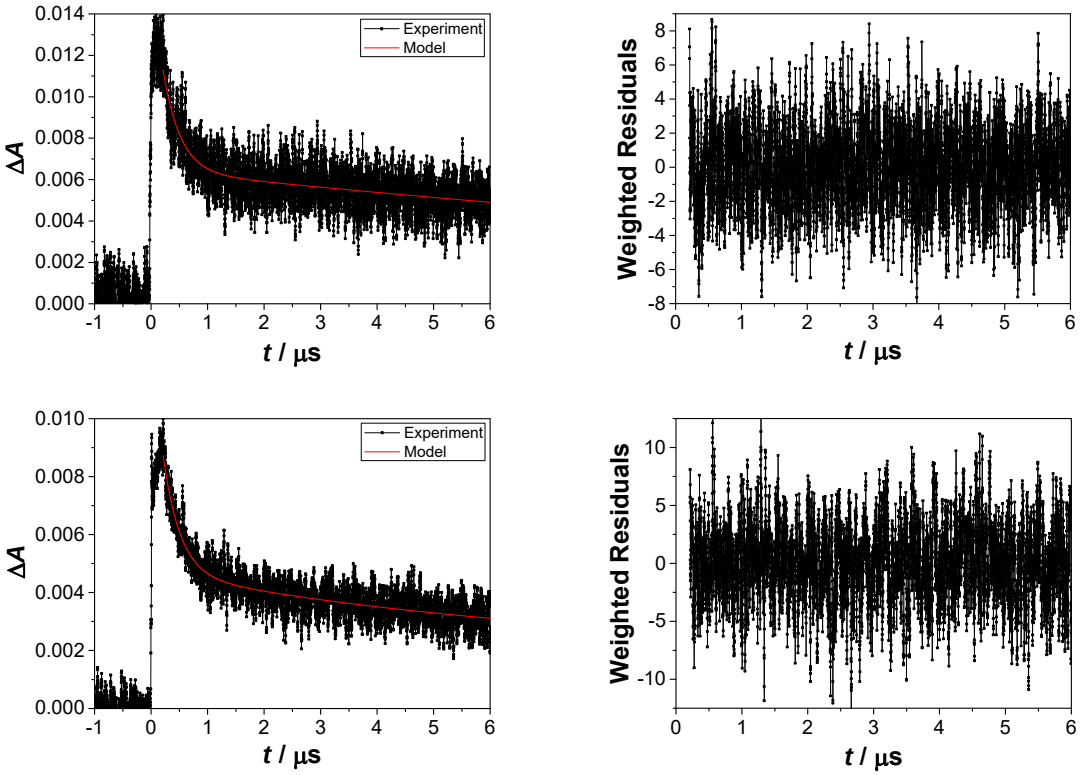

Fig S26. Decay of transient absorbance at 330 nm (top left) and 400 nm (bottom left) and their corresponding weighted residuals (top right and bottom right) for N_2-purged CH_3CN-H_2O (1:1 - v/v) solution of **1** in the presence of phosphate buffer (c = 0.05 mol dm^{-3}) at pH 7. E_{laser} = 20 mJ.

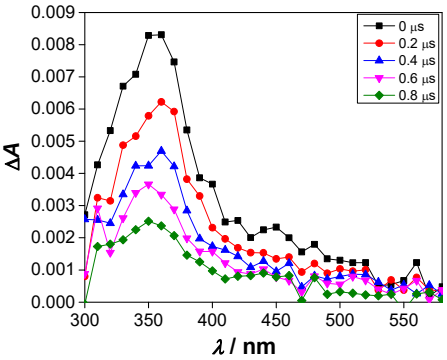

Fig S27. Transient absorption spectra of **2** ($c = 3.50 \times 10^{-4}$ mol dm^{-3}) in N_2-purged CH_3CN. E_{laser} = 12 mJ. A_{266} = 0.4.

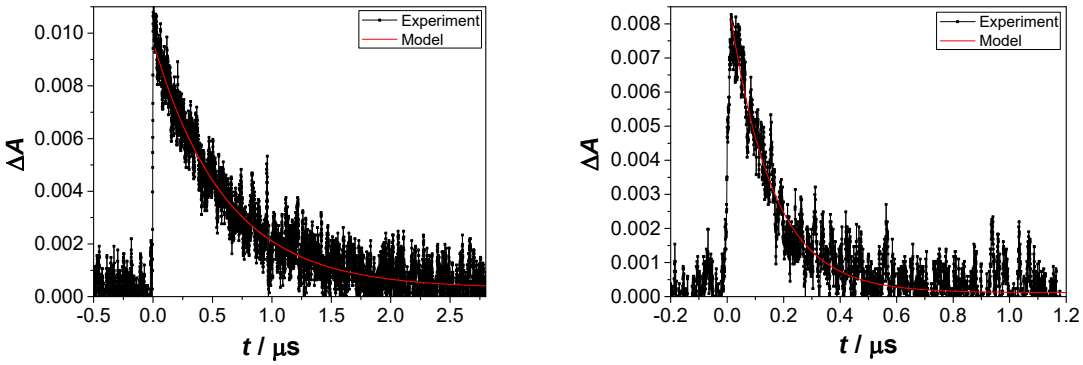

Fig S28. Decay of transient absorbance at 360 nm in N_2-purged (left) and non-purged (right) solution of **2** in CH_3CN. E_{laser} = 8 mJ.

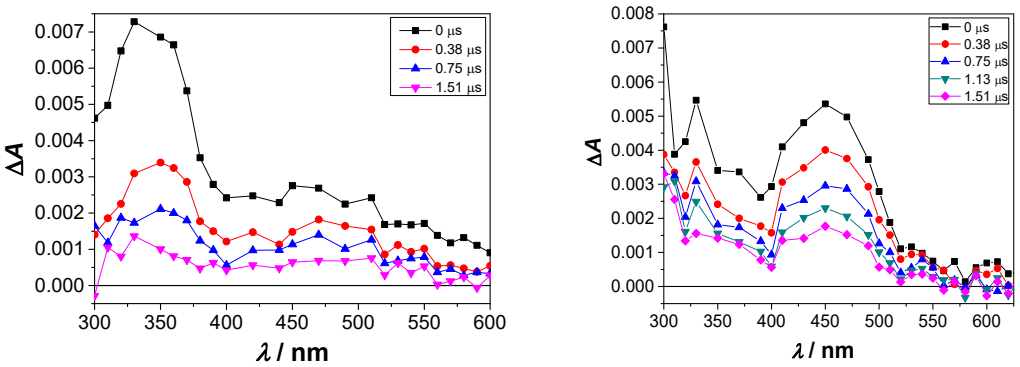

Fig S29. Transient absorption spectra of **2** (c = 2.16 × 10^{-4} mol dm^{-3} (pH 4); c = 1.62 × 10^{-4} mol dm^{-3} (pH 7)) in N_2-purged CH_3CN-H_2O (1:1 - v/v) in the presence of phosphate buffer (c = 0.05 mol dm^{-3}) at pH 4 (left) and pH 7 (right). E_{laser} = 20 mJ.

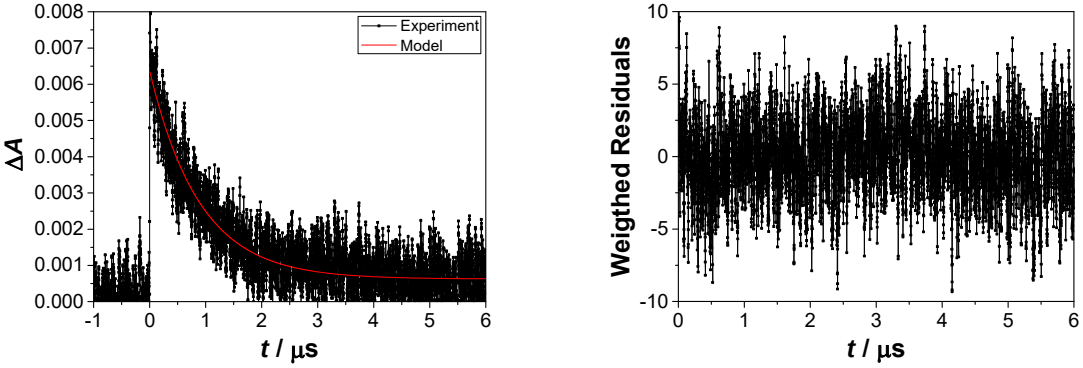

Fig S30. Decay of transient absorbance at 350 nm for N_2-purged CH_3CN-H_2O (1:1 - v/v) solution of **2** in the presence of phosphate buffer (c = 0.05 mol dm^{-3}) at pH 4 (left) and the corresponding weighted residuals (right). E_{laser} = 20 mJ.

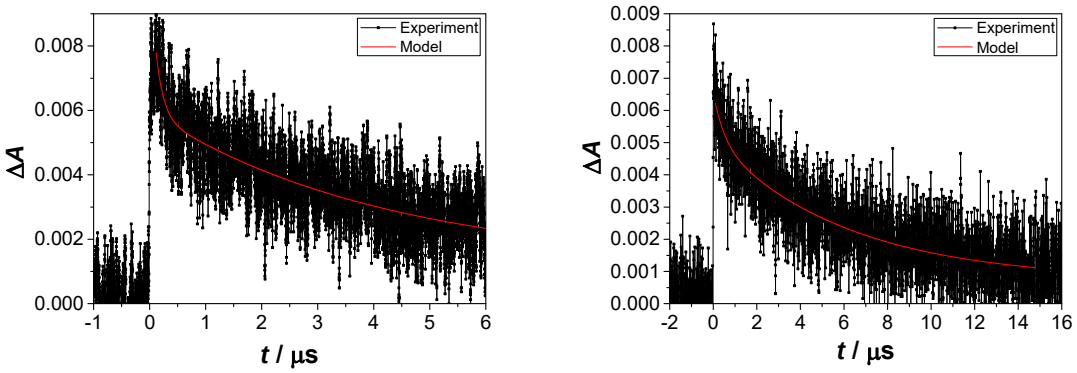

Fig S31. Decay of transient absorbance at 330 nm for N_2-purged CH_3CN-H_2O (1:1 - v/v) solution of **2** in the presence of phosphate buffer (c = 0.05 mol dm^{-3}) at pH 7, at two different time-scales. E_{laser} = 20 mJ.

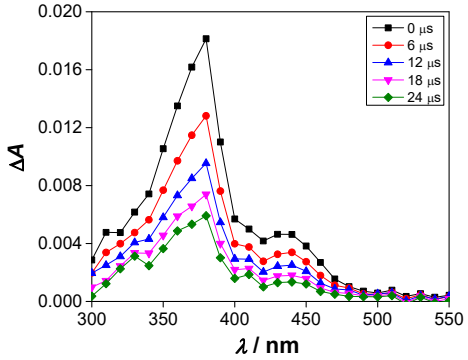

Fig S32. Transient absorption spectra of **3** (c = 2.84 × 10^{-4} mol dm^{-3}) in N_2 purged CH_3CN. E_{laser} = 8 mJ. A_{266} = 0.46.

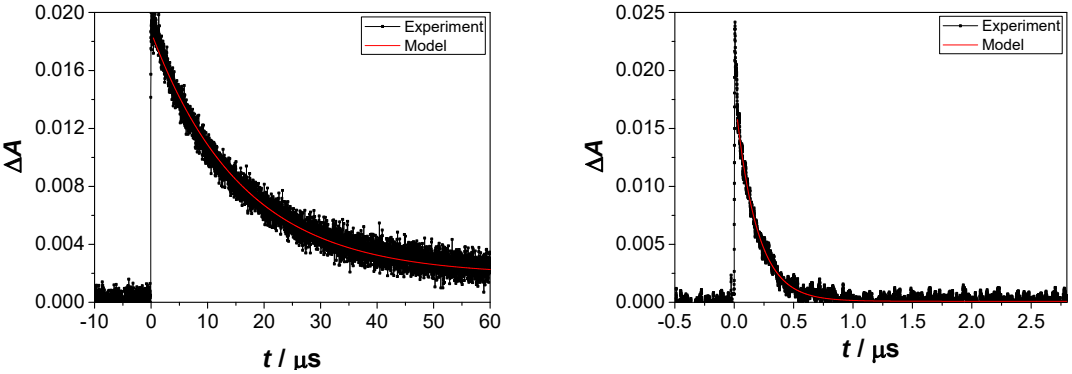

Fig S33. Decay of transient absorbance at 390 nm for N_2-purged (left) and non-purged (right) CH_3CN solution of **3**. E_{laser} = 8 mJ.

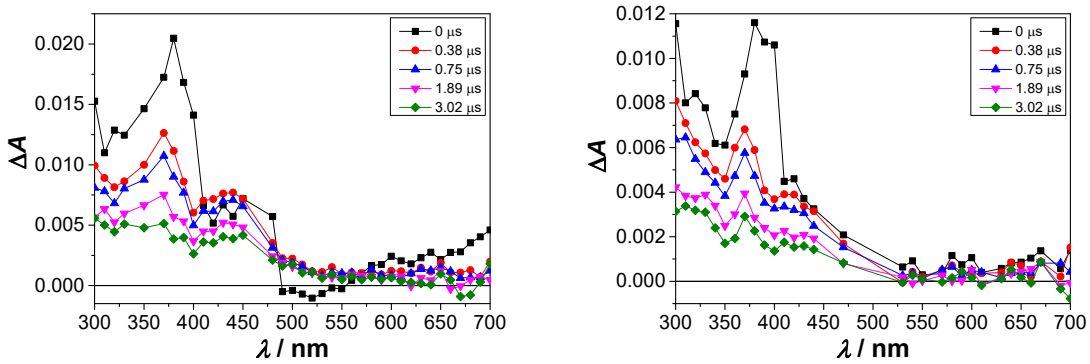

Fig S34. Transient absorption spectra of **3** (c = 1.05 × 10^{-4} mol dm^{-3} (pH 4); c = 7.55 × 10^{-5} mol dm^{-3} (pH 7)) in N_2-purged CH_3CN-H_2O (1:1 - v/v) in the presence of phosphate buffer (c = 0.05 mol dm^{-3}) at pH 4 (left) and pH 7 (right). E_{laser} = 20 mJ.

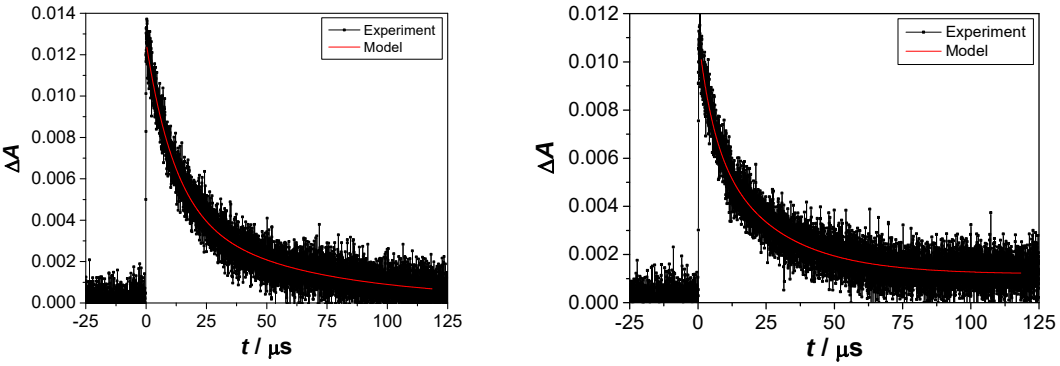

Fig S35. Decay of transient absorbance at 380 nm for N_2-purged CH_3CN-H_2O (1:1 - v/v) solution of **3** in the presence of phosphate buffer (c = 0.05 mol dm^{-3}) at pH 4 (left) and pH 7 (right). E_{laser} = 20 mJ.

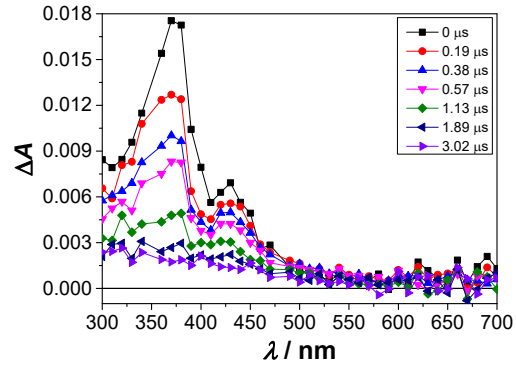

Fig S36. Transient absorption spectra of **4** (c = 1.89 × 10^{-4} mol dm^{-3}) in N_2-purged CH_3CN. E_{laser} = 8 mJ.

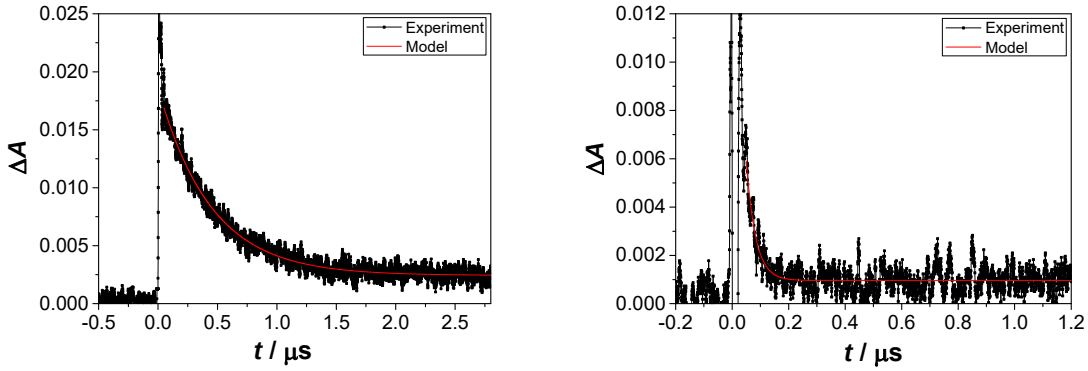

Fig S37. Decay of transient absorbance at 380 nm for N_2-purged (left) and O_2-purged (right) CH_3CN solution of **4**. E_{laser} = 8 mJ.

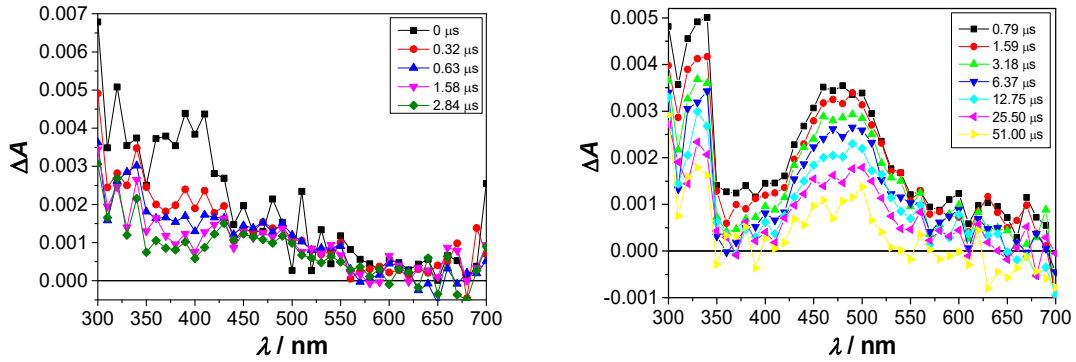

Fig S38. Transient absorption spectra of **4** (c = 1.35 × 10^{-4} mol dm^{-3} (pH 4); c = 4.53 × 10^{-5} mol dm^{-3} (pH 7)) in N_2-purged CH_3CN-H_2O (1:1 - v/v) in the presence of phosphate buffer (c = 0.05 mol dm^{-3}) at pH 4 (left) and pH 7 (right). E_{laser} = 20 mJ.

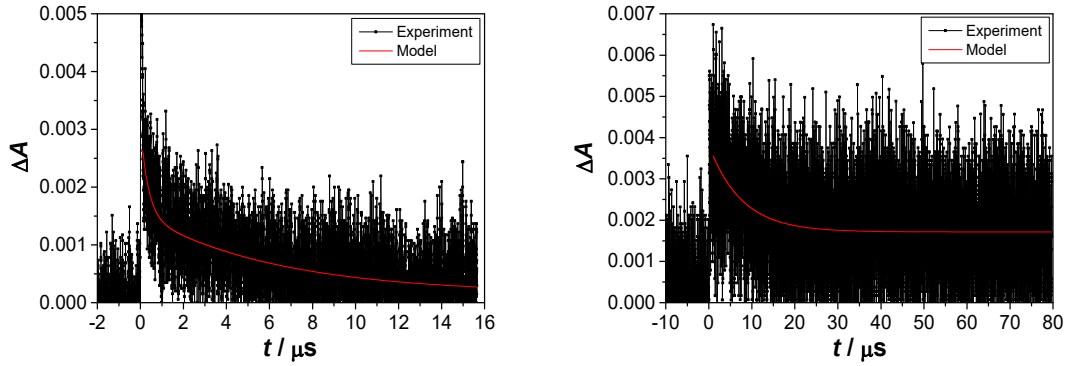

Fig S39. Decay of transient absorbance at 380 nm for N_2-purged CH_3CN-H_2O (1:1 - v/v) solution of **4** in the presence of phosphate buffer (c = 0.05 mol dm^{-3}) at pH 4 (left) and pH 7 (right). E_{laser} = 20 mJ.

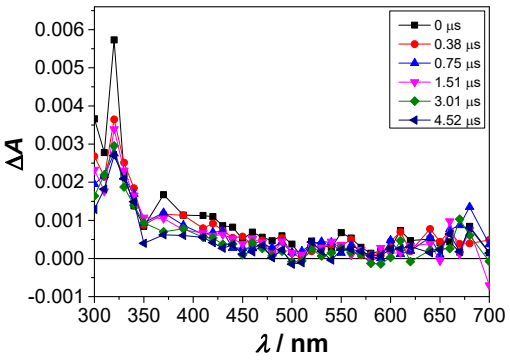

Fig S40. Transient absorption spectra of **5** (c = 3.24 × 10^{-5} mol dm^{-3}) in N_2-purged CH_3CN. E_{laser} = 20 mJ.

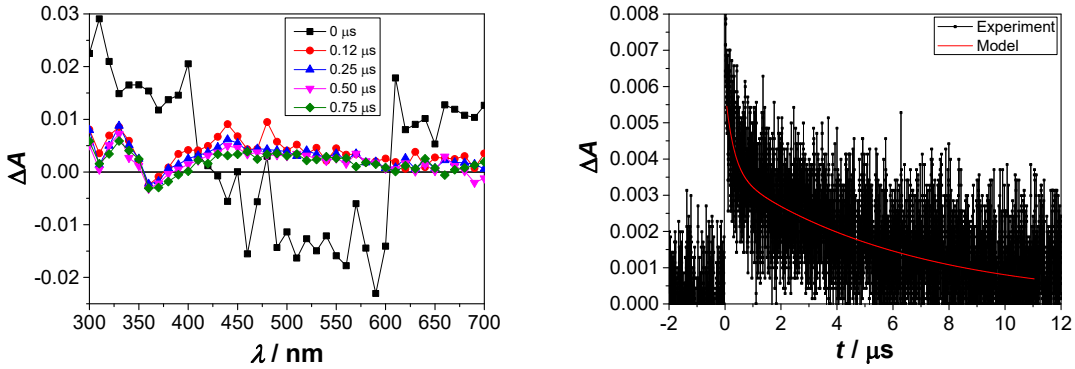

Fig S41. Transient absorption spectra of **6** (c = 1.74 × 10^{-5} mol dm^{-3}) in N_2-purged CH_3CN (left) and decay of transient absorbance at 330 nm (right). E_{laser} = 20 mJ.

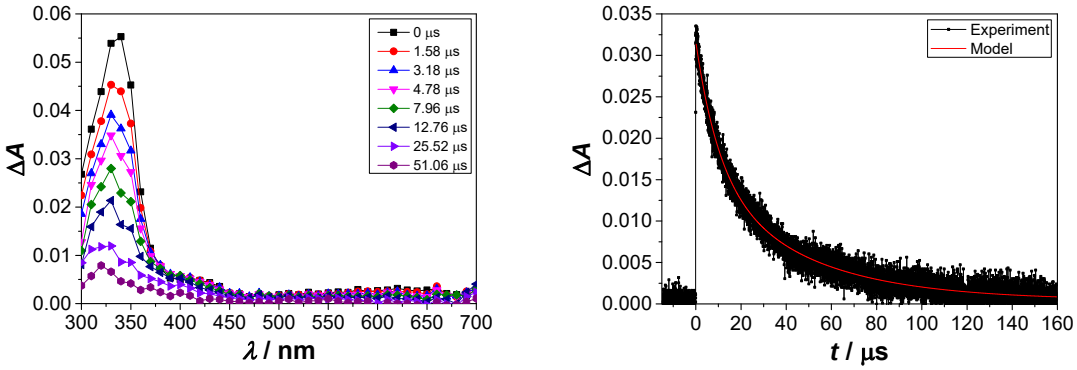

Fig S42. Transient absorption spectra of *N*-methylphthalimide (c = 5.37 × 10^{-4} mol dm^{-3}) in N_2-purged CH_3CN-H_2O (1:1 - v/v) in the presence of phosphate buffer (c = 0.05 mol dm^{-3}) at pH 4 (left) and decay of transient absorbance at 330 nm (right). The decay was fit to a sum of two exponentials with decay times of τ = 10.6 ± 0.4 μs and τ = 46 ± 3 μs. E_{laser} = 8 mJ.

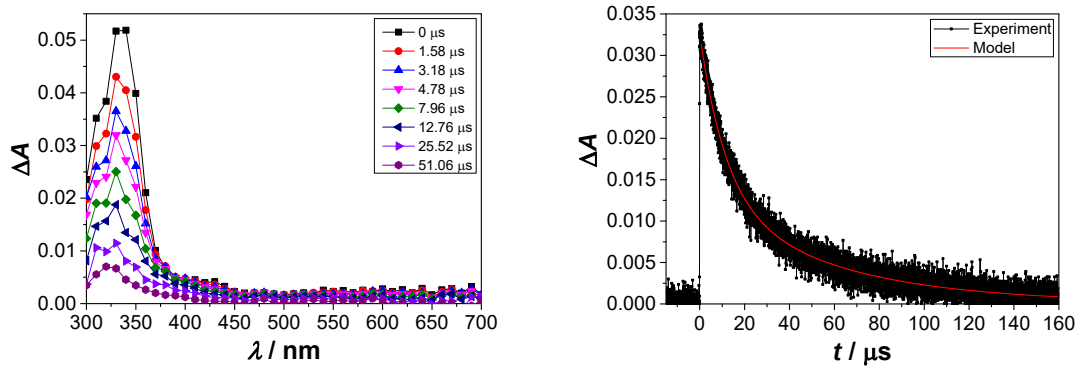

Fig S43. Transient absorption spectra of *N*-methylphthalimide (c = 5.37 × 10^{-4} mol dm^{-3}) in N_2-purged CH_3CN-H_2O (1:1 - v/v) in the presence of phosphate buffer (c = 0.05 mol dm^{-3}) at pH 7 (left) and decay of transient absorbance at 330 nm (right). The decay was fit to a sum of two exponentials with decay times of τ = 10.7 ± 0.7 µs and τ = 51 ± 4 µs. E_{laser} = 8 mJ.

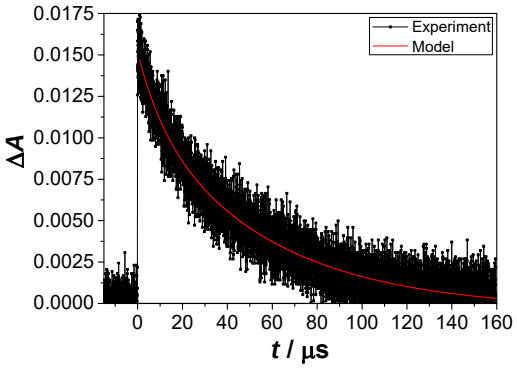

Fig S44. Decay of transient absorption for *N*-methylphthalimide (c = 5.37 × 10^{-4} mol dm^{-3}) in N_2-purged CH_3CN-H_2O (1:1 - v/v) in the absence of buffer The decay was fit to a sum of two exponentials with decay times of τ = 12 ± 2 µs and τ = 54 ± 3 µs. E_{laser} = 8 mJ.

6. MS and NMR Spectra

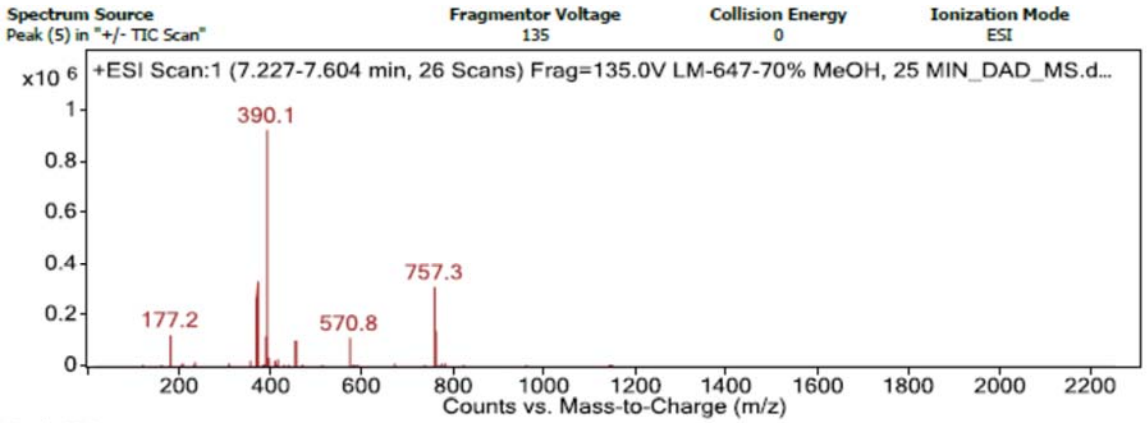

Peak List

m/z	z	Abund
177.2		121382.2
368.2	1	332144.1
369.2	1	78268.6
387.2		113553.2
390.1	1	922399.6
391.2	1	221620
452.1		101518
570.8		108351.3
757.3	1	307876.8
758.3	1	138800.6

Fig S45. Mass spectrum of **2COCH$_3$** (obtained by photolysis of **2** in CH_3CN-H_2O (2:1 - v/v)).

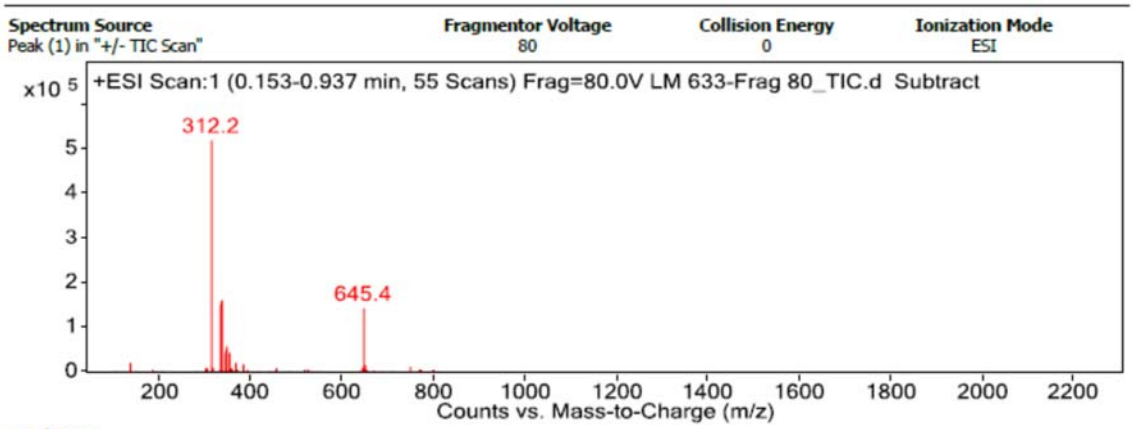

Peak List

m/z	z	Abund
312.2	1	519948.6
313.2	1	117639.1
334.2	1	161867.1
335.2	1	33731.9
344.3		60630.5
353.3		42820.7
645.4	1	141851.6
646.4	1	51979.3

Fig S46. Mass spectrum of **3H** (obtained by photolysis of **3** in CH_3CN-H_2O (3:1 - v/v)).

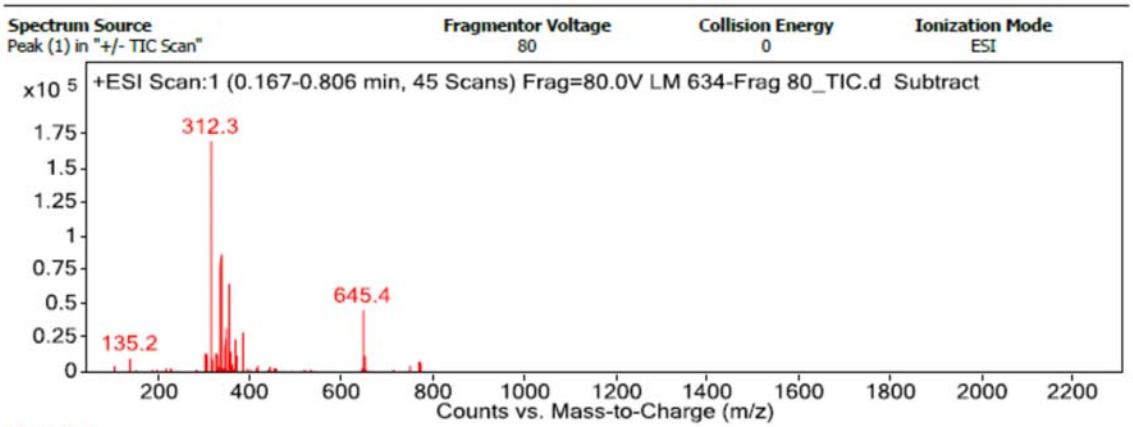

Peak List

m/z	z	Abund
312.3	1	170493.1
313.3	1	76313.1
334.2	1	87300.4
335.2	1	34859.6
344.3		32423
353.4	1	65351.8
366.2	1	24678.3
381.4		30084.1
645.4	1	45788.1
646.4	1	31387.4

Fig S47. Mass spectrum of **3H/3D** (obtained by photolysis of **3** in CH_3CN-D_2O (3:1 - v/v)).

Fig S48. ^{1}H (DMSO-d_6, 600 MHz) NMR spectrum of **2**.

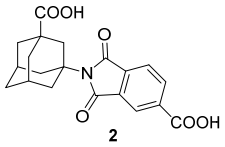

2

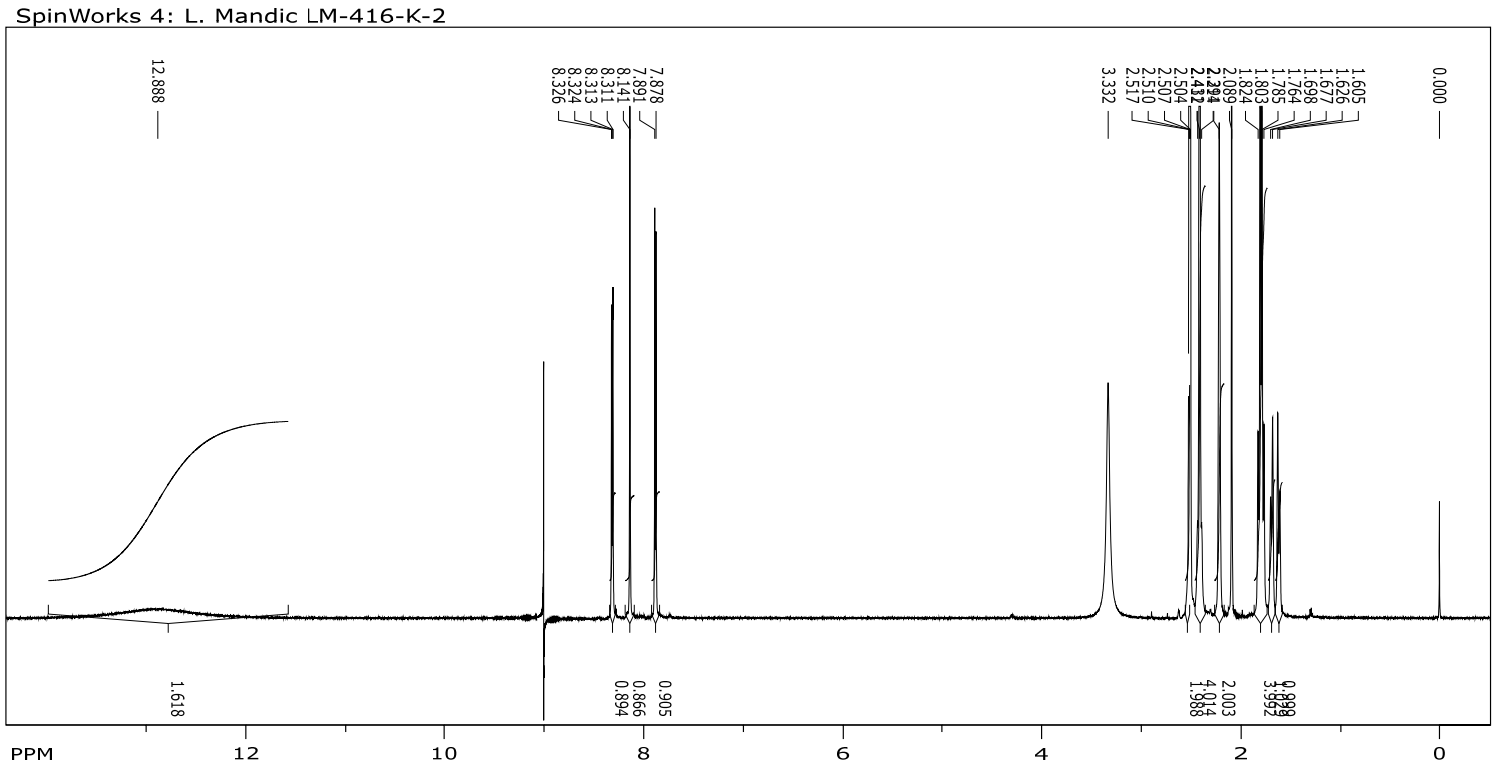

file: ...:\NMR (AntiVir)\Compound 15\1H\fid expt: <zg30>
transmitter freq.: 600.135401 MHz
time domain size: 32768 points
width: 12019.23 Hz = 20.0275 ppm = 0.366798 Hz/pt
number of scans: 19

freq. of 0 ppm: 600.129995 MHz
processed size: 32768 complex points
LB: 0.300 GF: 0.0000

Fig S49. ^{13}C (DMSO-d_6, 150 MHz, APT) NMR spectrum of **2**.

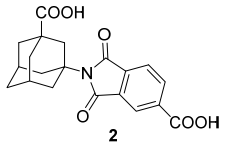

2

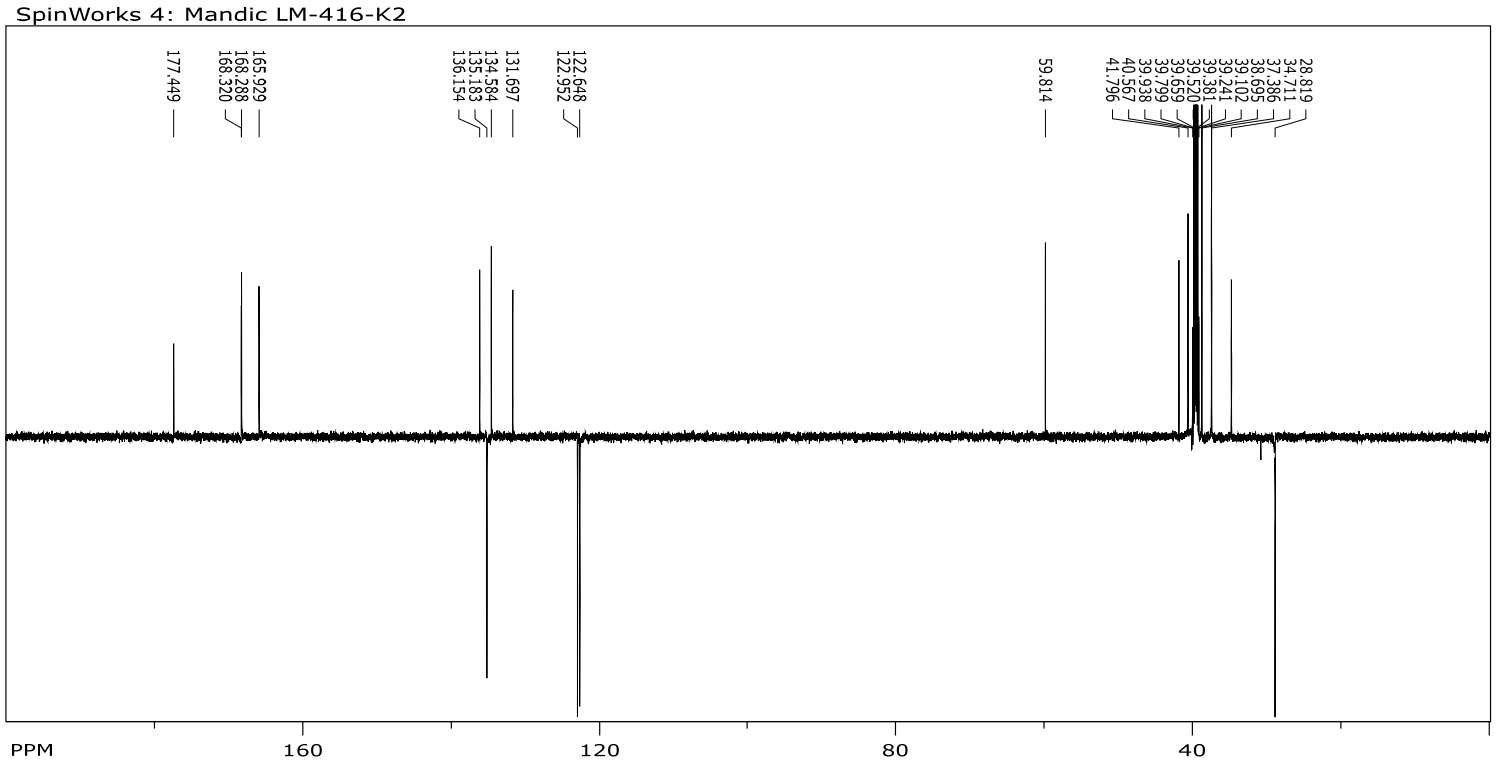

file: ...a\3-(4'-COOH)PhthAd-1-COOH\APT\fid expt: <jmod>
transmitter freq.: 150.917899 MHz
time domain size: 65536 points
width: 39370.08 Hz = 260.8708 ppm = 0.600740 Hz/pt
number of scans: 2249

freq. of 0 ppm: 150.902871 MHz
processed size: 32768 complex points
LB: 1.000 GF: 0.0000

Fig S50. ^{1}H (DMSO-d_6, 300 MHz) NMR spectrum of **3**.

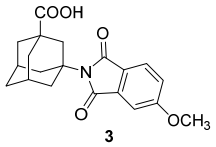

3

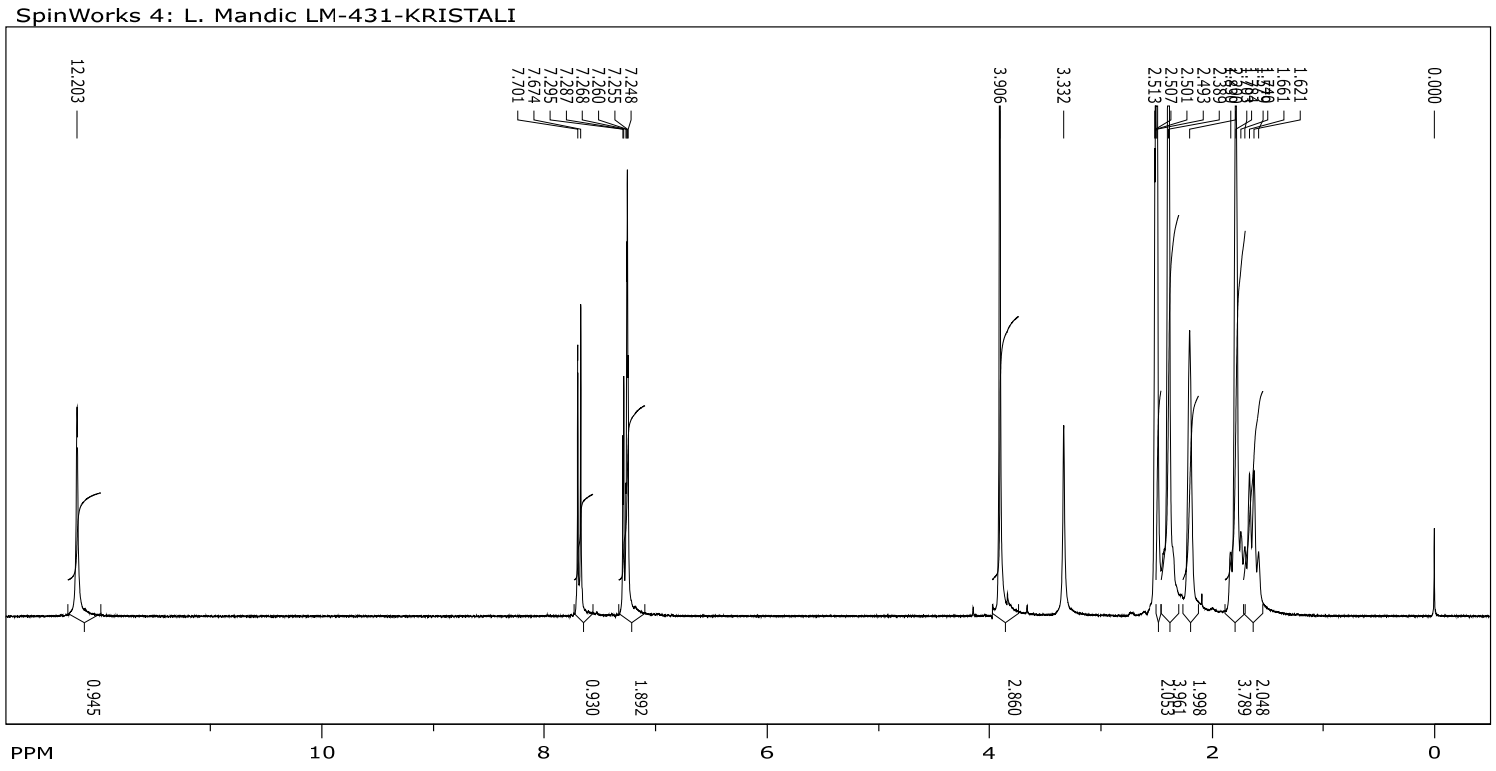

file: ...:\NMR (AntiVir)\Compound 13\1H\fid expt: <zg30>
transmitter freq.: 300.132701 MHz
time domain size: 32768 points
width: 6172.84 Hz = 20.5670 ppm = 0.188380 Hz/pt
number of scans: 28

freq. of 0 ppm: 300.129999 MHz
processed size: 32768 complex points
LB: 0.300 GF: 0.0000

Fig S51. ^{13}C (DMSO-d_6, 150 MHz, APT) NMR spectrum of **3**.

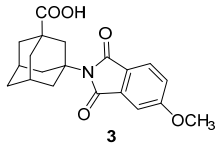

3

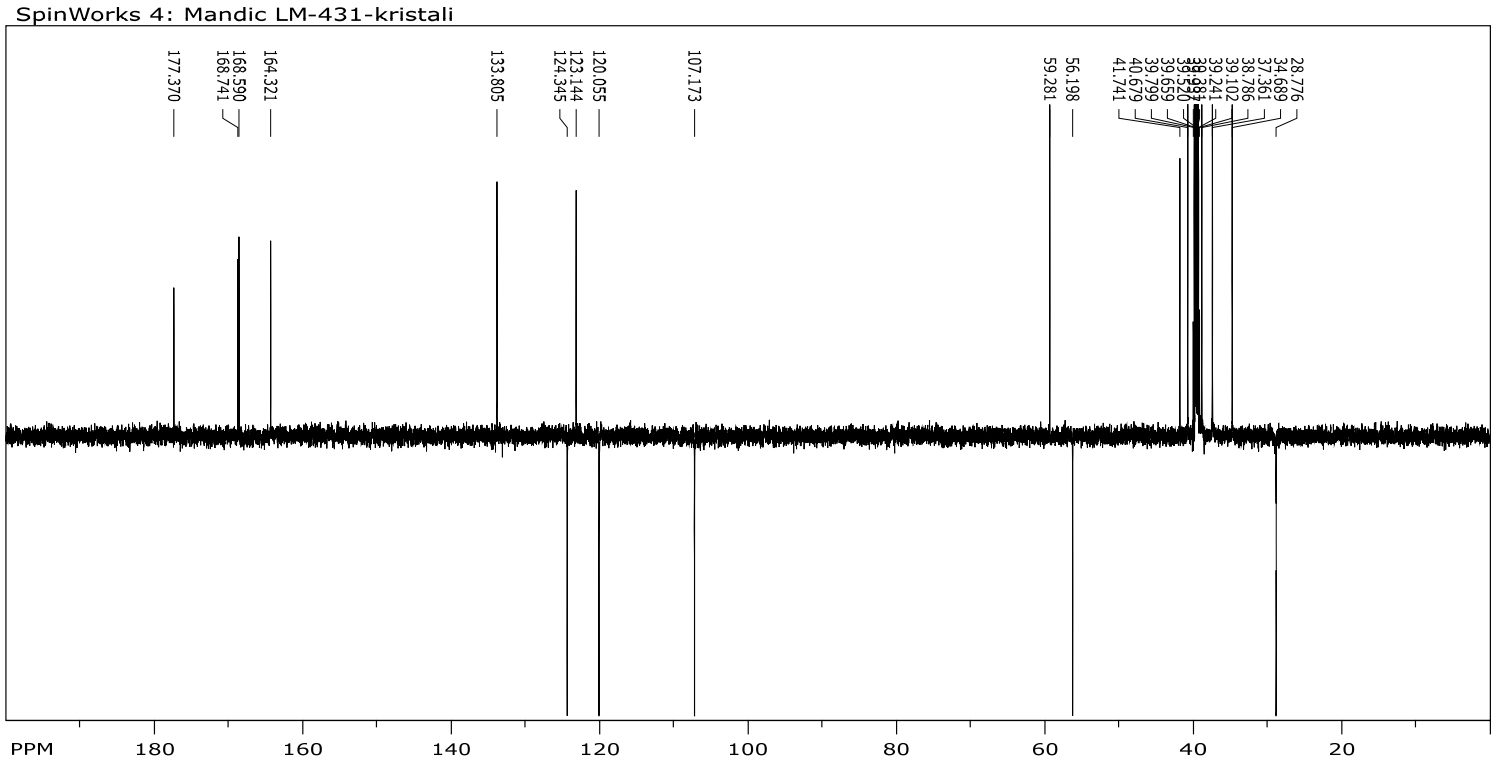

Fig S52. ^{1}H (DMSO-d_6, 300 MHz) NMR spectrum of **4**.

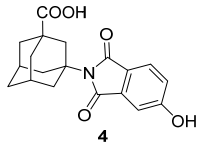

4

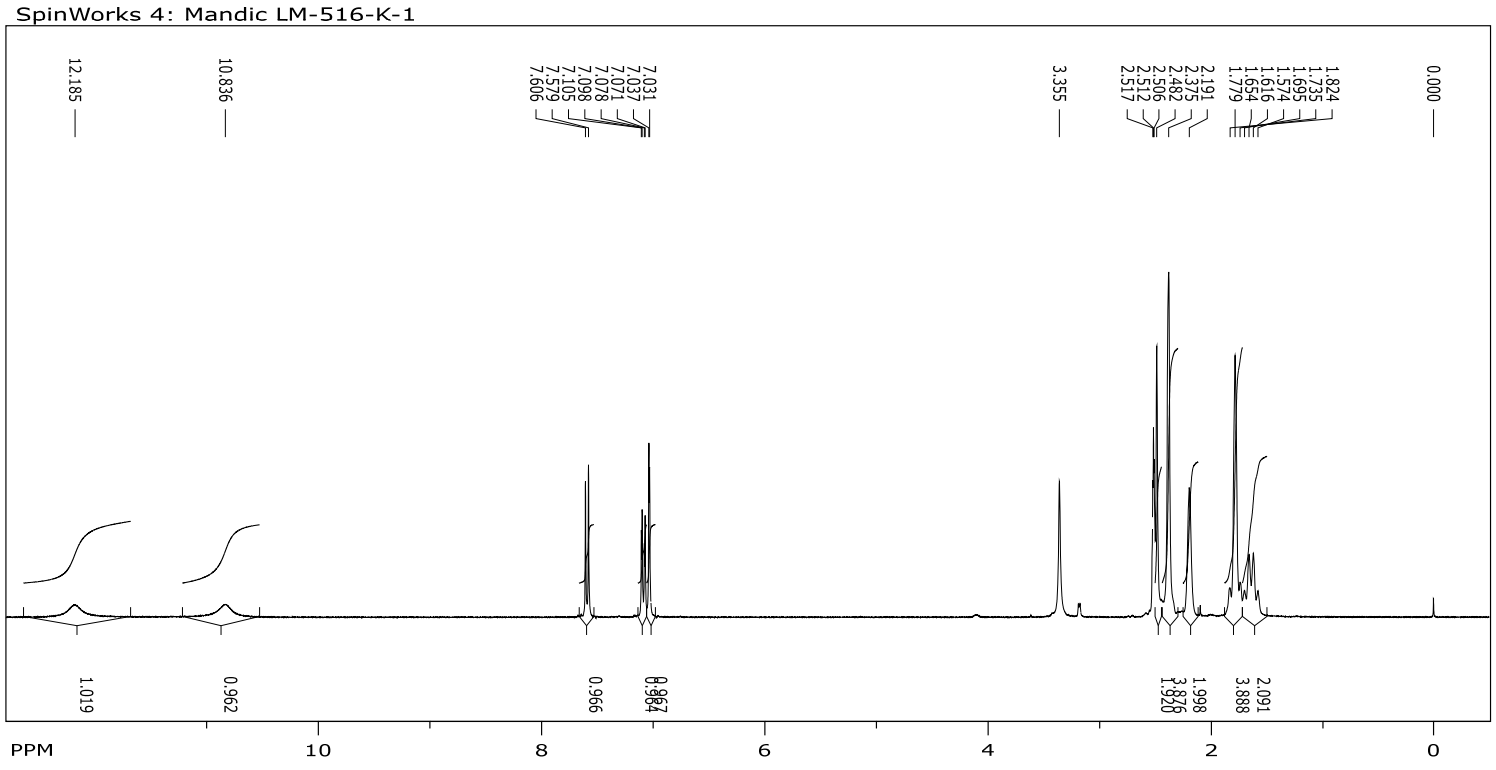

file: ...\NMR (SubstPhth)\Compound 4\1H\fid expt: <zg30>
transmitter freq.: 300.132701 MHz
time domain size: 32768 points
width: 6172.84 Hz = 20.5670 ppm = 0.188380 Hz/pt
number of scans: 14

freq. of 0 ppm: 300.129998 MHz
processed size: 32768 complex points
LB: 0.300 GF: 0.0000

Fig S53. ^{13}C (DMSO-d_6, 75 MHz, COM) NMR spectrum of **4**.

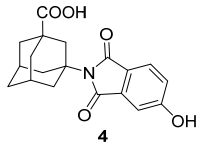

4

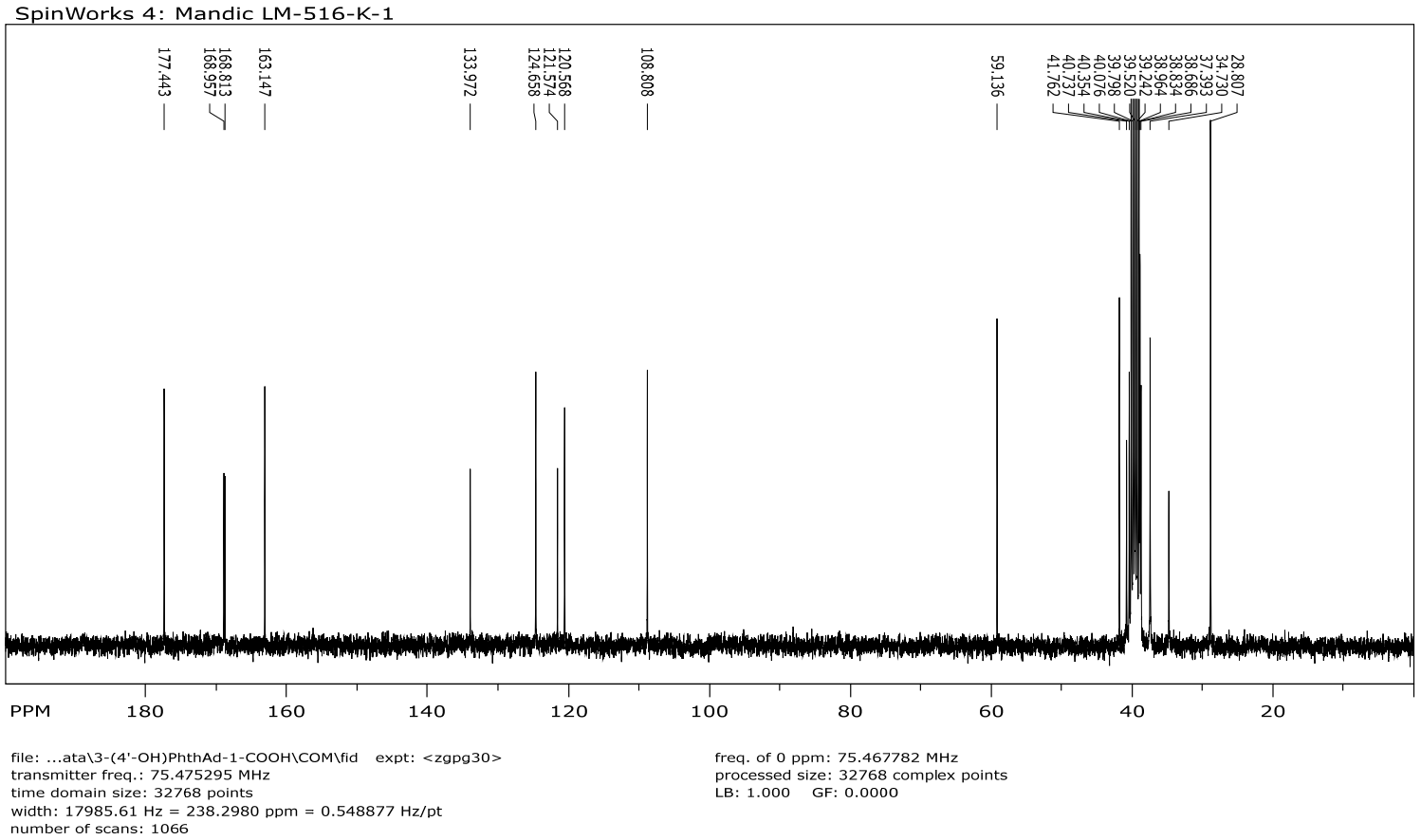

Fig S54. ^{1}H (DMSO-d_6, 300 MHz) NMR spectrum of **5**.

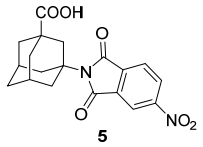

5

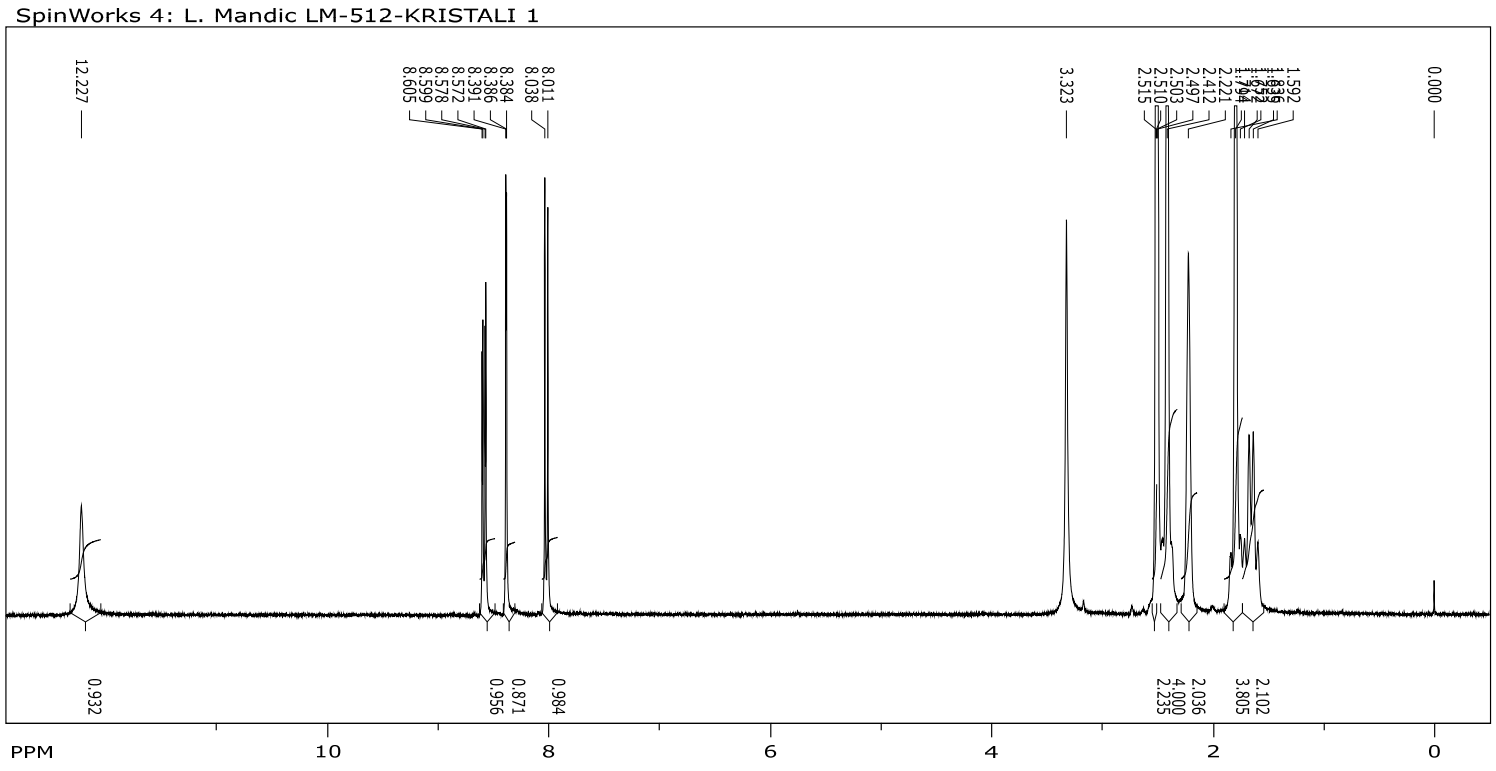

file: ...:\NMR (AntiVir)\Compound 11\1H\fid expt: <zg30>
transmitter freq.: 300.132701 MHz
time domain size: 32768 points
width: 6172.84 Hz = 20.5670 ppm = 0.188380 Hz/pt
number of scans: 12

freq. of 0 ppm: 300.130000 MHz
processed size: 32768 complex points
LB: 0.300 GF: 0.0000

Fig S55. ^{13}C (DMSO-d_6, 75 MHz, COM) NMR spectrum of **5**.

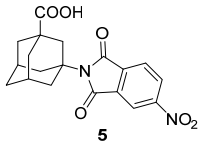

5

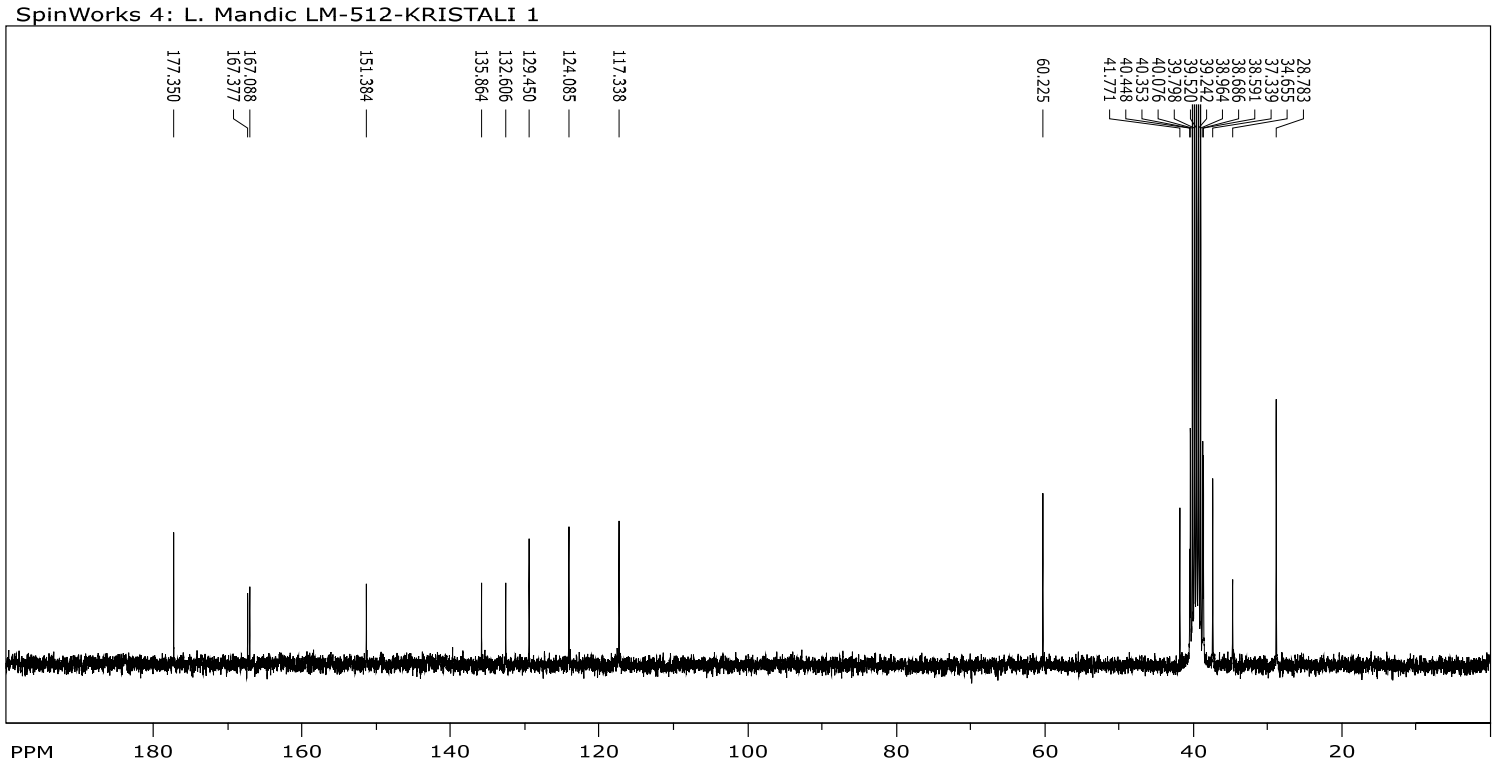

Fig S56. ^{1}H (CD_3OD, 300 MHz) NMR spectrum of **6**.

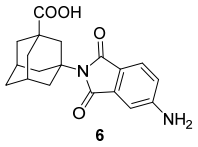

6

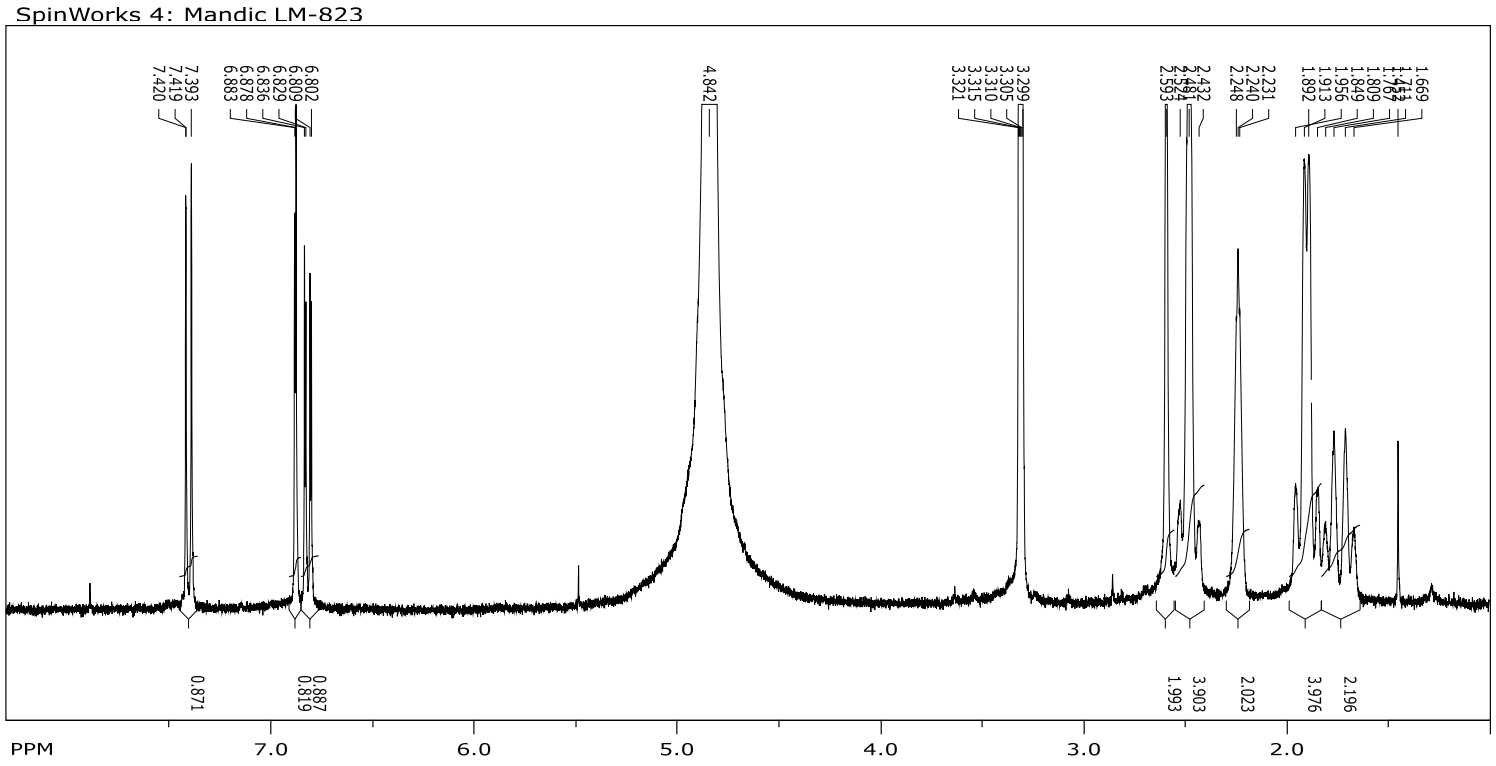

file: ...:\NMR (AntiVir)\Compound 12\1H\fid expt: <zg30>
transmitter freq.: 300.132701 MHz
time domain size: 32768 points
width: 6172.84 Hz = 20.5670 ppm = 0.188380 Hz/pt
number of scans: 20

freq. of 0 ppm: 300.130005 MHz
processed size: 32768 complex points
LB: 0.000 GF: 0.0000

Fig S57. ^{13}C (CD_3OD, 75 MHz, APT) NMR spectrum of **6**.

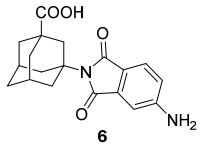

6

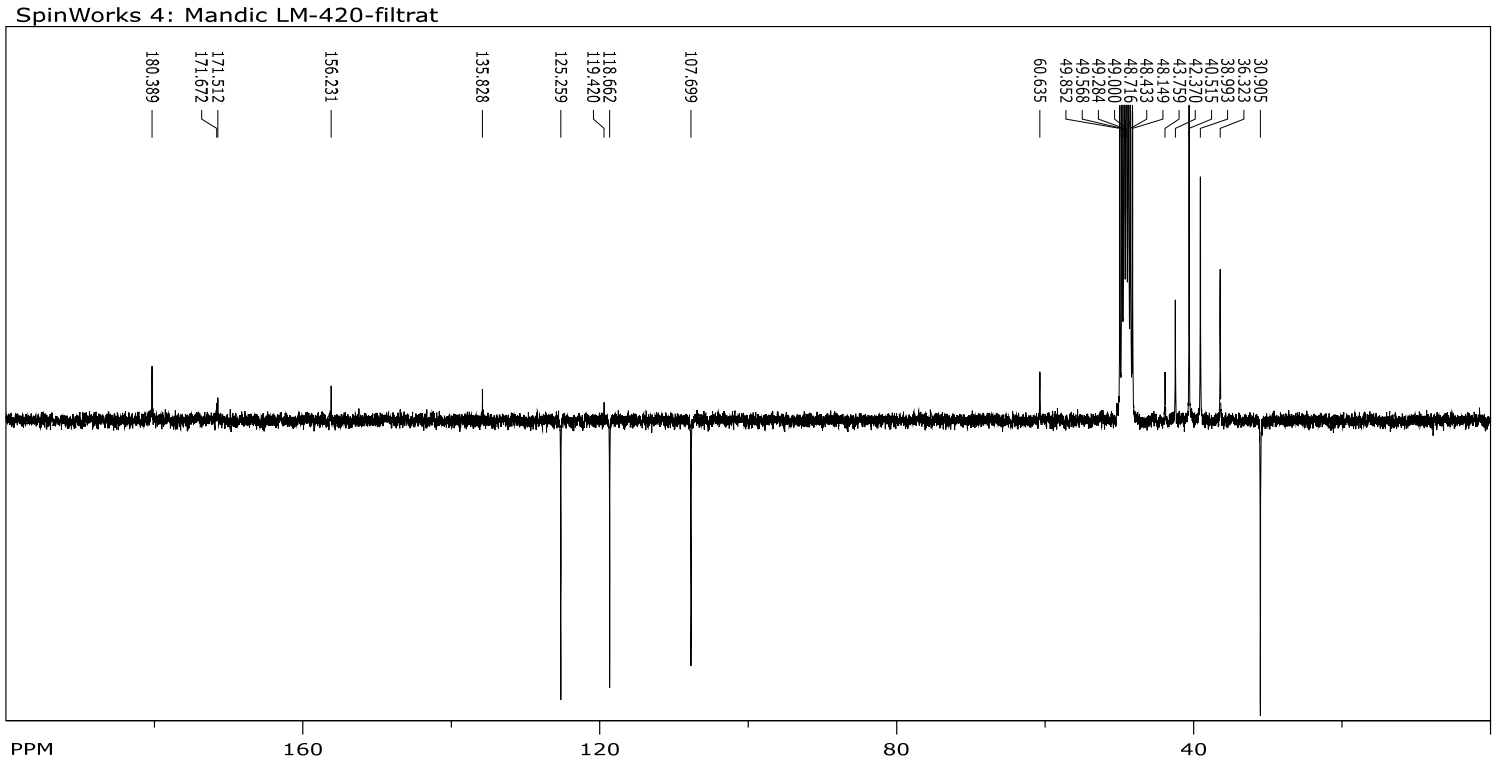

Fig S58. ^{1}H (DMSO-d_6, 600 MHz) NMR spectrum of **2H**.

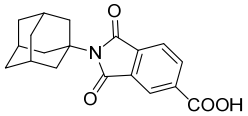

2H

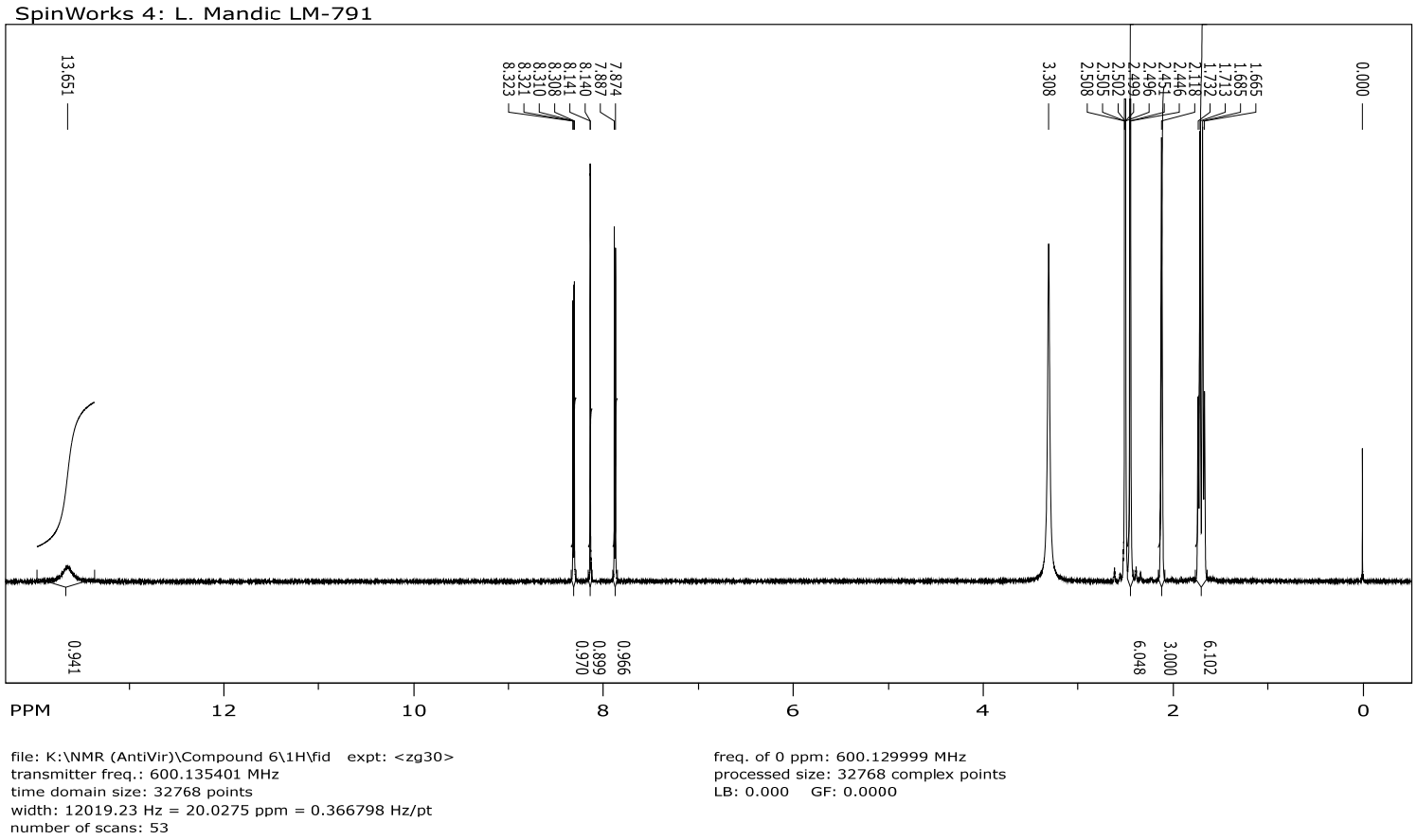

file: K:\NMR (AntiVir)\Compound 6\1H\fid expt: <zg30>
transmitter freq.: 600.135401 MHz
time domain size: 32768 points
width: 12019.23 Hz = 20.0275 ppm = 0.366798 Hz/pt
number of scans: 53

freq. of 0 ppm: 600.129999 MHz
processed size: 32768 complex points
LB: 0.000 GF: 0.0000

Fig S59. ^{13}C (DMSO-d_6, 150 MHz, APT) NMR spectrum of **2H**.

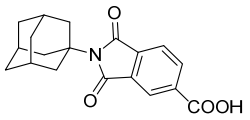

2H

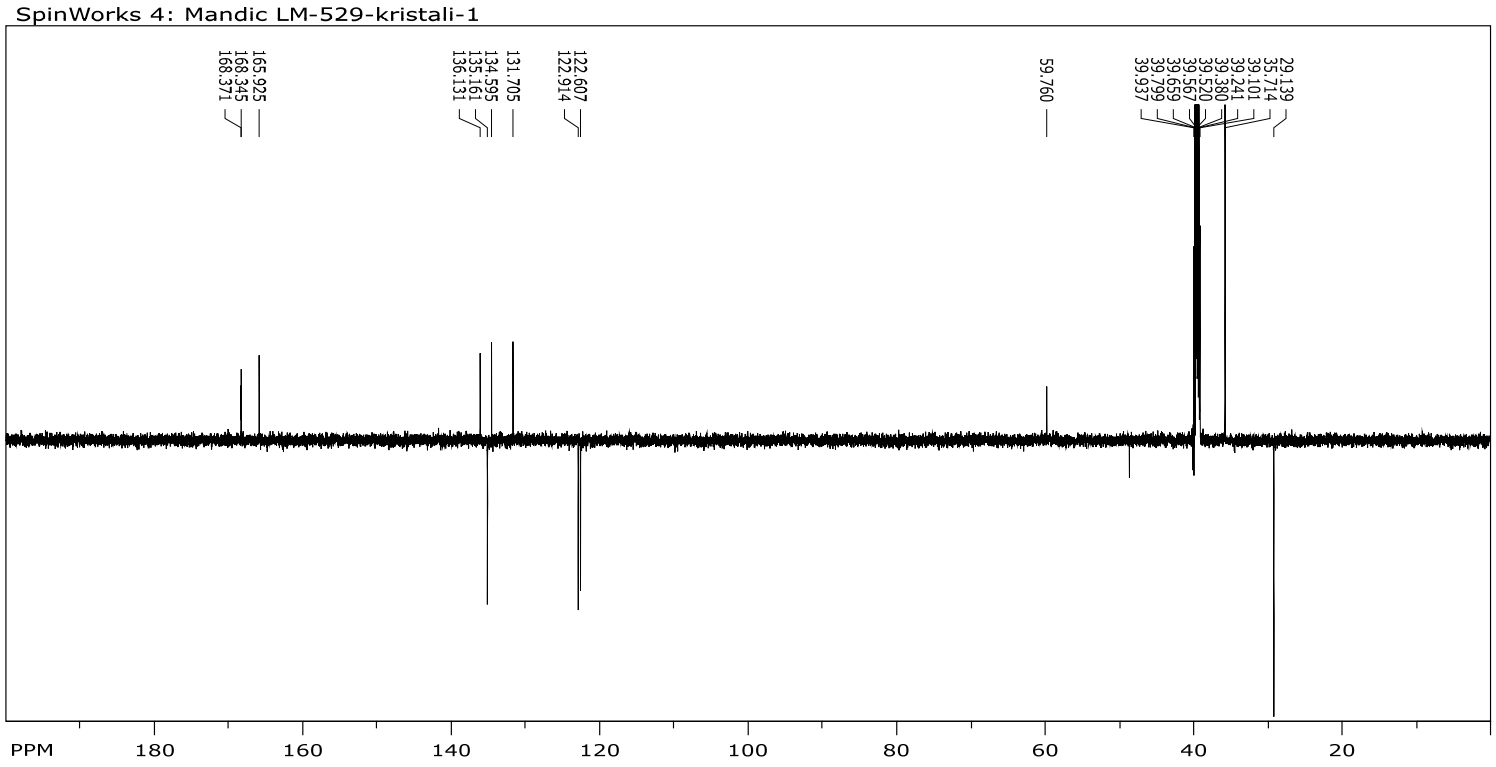

Fig S60. ^{1}H (DMSO-d_6, 600 MHz) NMR spectrum of **3H**.

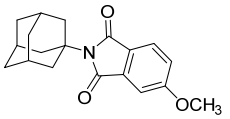

3H

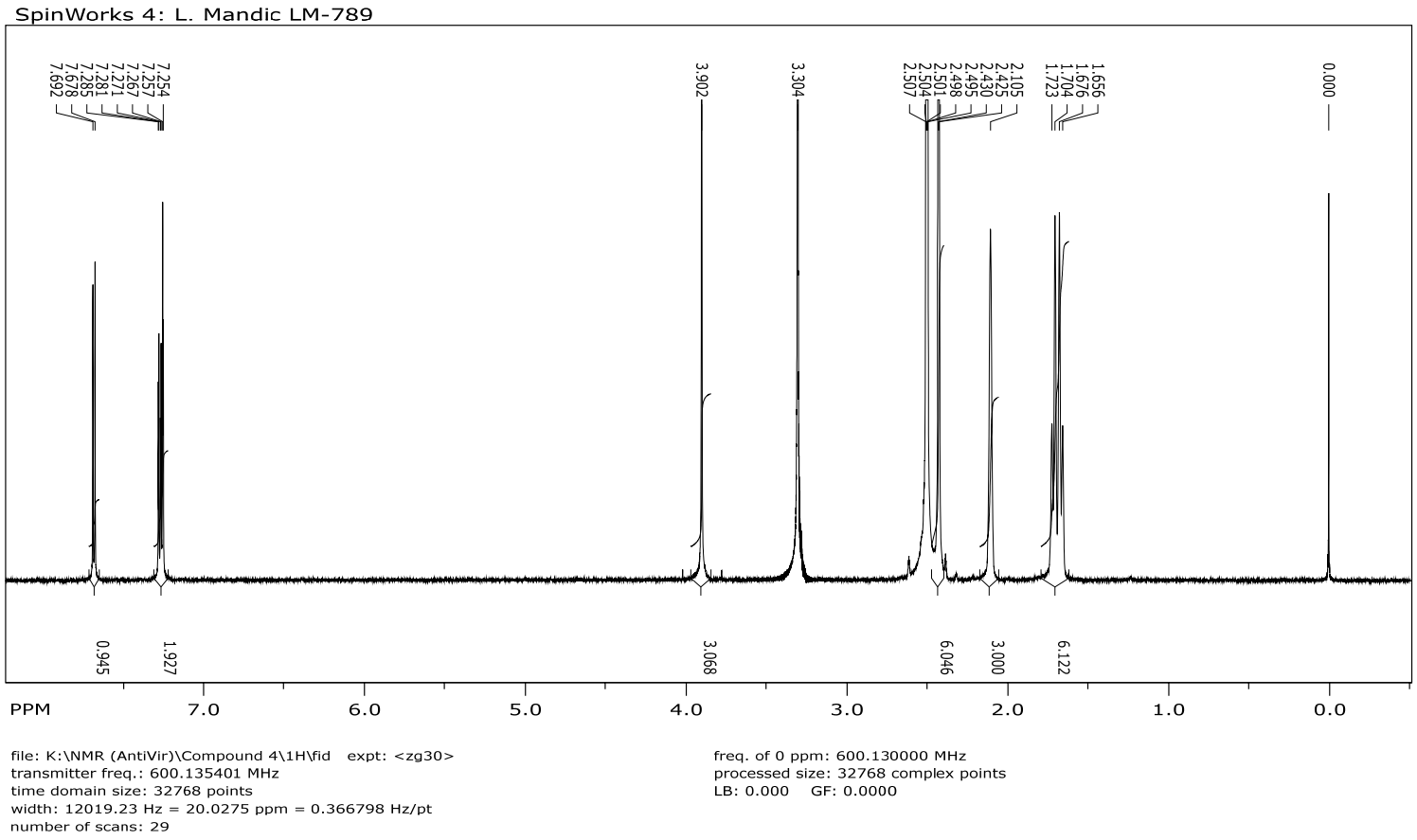

file: K:\NMR (AntiVir)\Compound 4\1H\fid expt: <zg30>
transmitter freq.: 600.135401 MHz
time domain size: 32768 points
width: 12019.23 Hz = 20.0275 ppm = 0.366798 Hz/pt
number of scans: 29

freq. of 0 ppm: 600.130000 MHz
processed size: 32768 complex points
LB: 0.000 GF: 0.0000

Fig S61. ^{13}C (DMSO-d_6, 75 MHz, COM) NMR spectrum of **3H**.

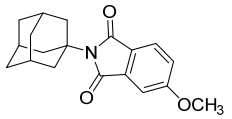

3H

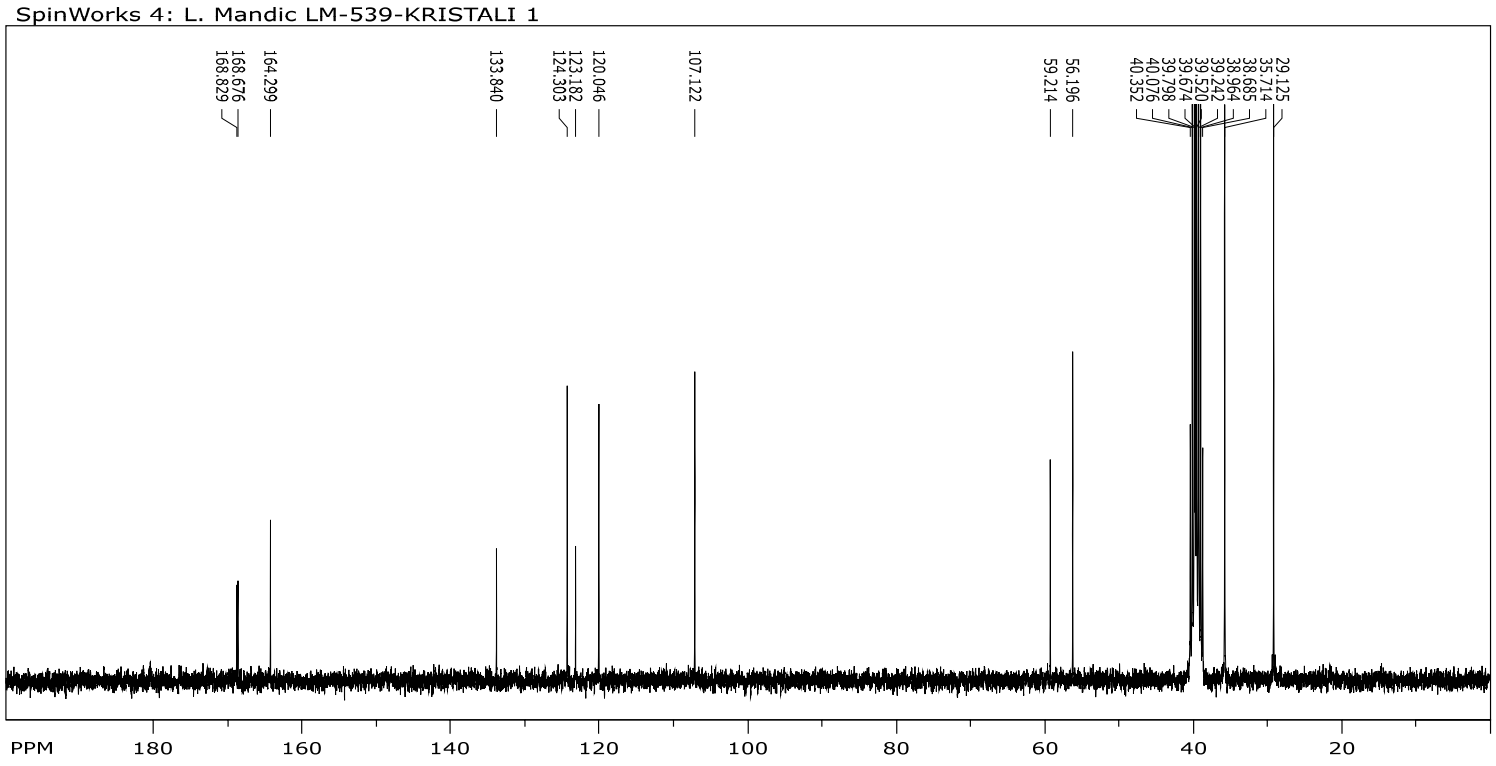

Fig S62. ^{1}H (DMSO-d_6, 600 MHz) NMR spectrum of **4H**.

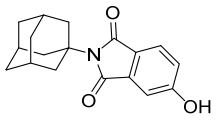

4H

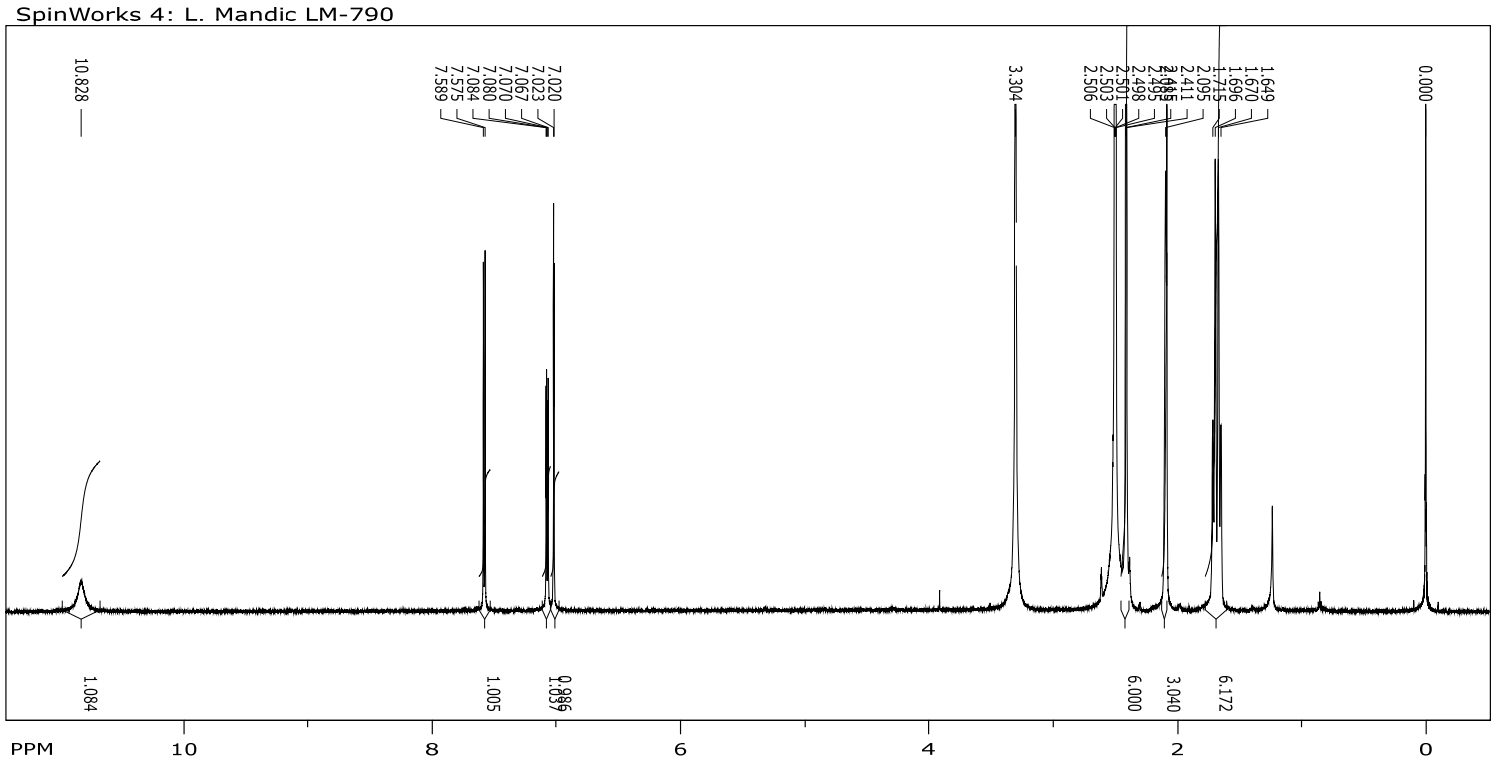

file: K:\NMR (AntiVir)\Compound 5\1H\fid expt: <zg30>
transmitter freq.: 600.135401 MHz
time domain size: 32768 points
width: 12019.23 Hz = 20.0275 ppm = 0.366798 Hz/pt
number of scans: 64

freq. of 0 ppm: 600.130000 MHz
processed size: 32768 complex points
LB: 0.000 GF: 0.0000

Fig S63. ^{13}C (DMSO-d_6, 75 MHz, COM) NMR spectrum of **4H**.

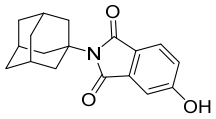

4H

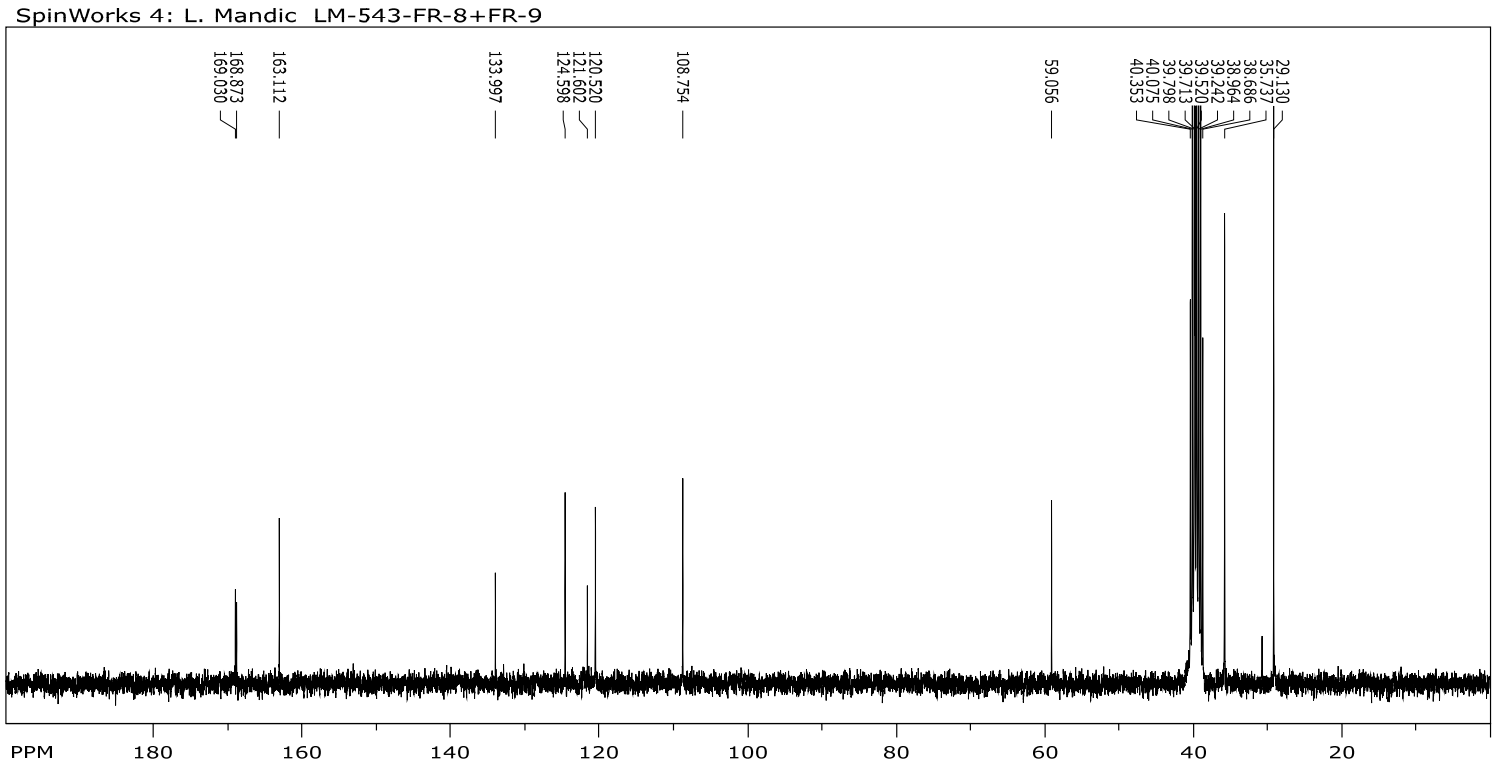

Fig S64. ^{1}H (DMSO-d_6, 600 MHz) NMR spectrum of **5H**.

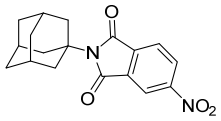

5H

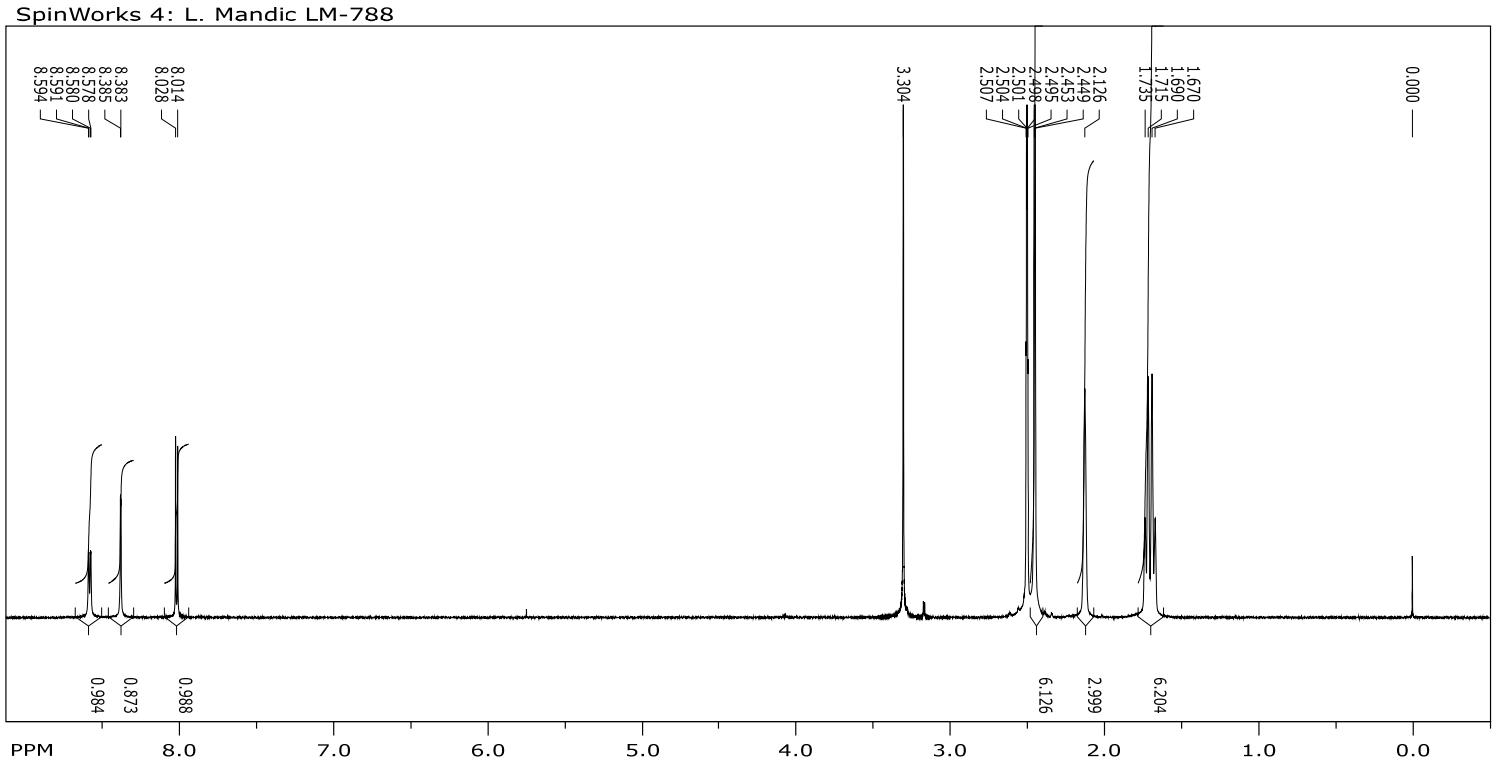

file: ...NMR (SubstPhth)\Compound 5H\1H\fid expt: <zg30>
transmitter freq.: 600.135401 MHz
time domain size: 32768 points
width: 12019.23 Hz = 20.0275 ppm = 0.366798 Hz/pt
number of scans: 37

freq. of 0 ppm: 600.130000 MHz
processed size: 32768 complex points
LB: 0.000 GF: 0.0000

Fig S65. ^{13}C (DMSO-d_6, 75 MHz, COM) NMR spectrum of **5H**.

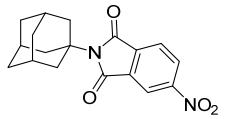

5H

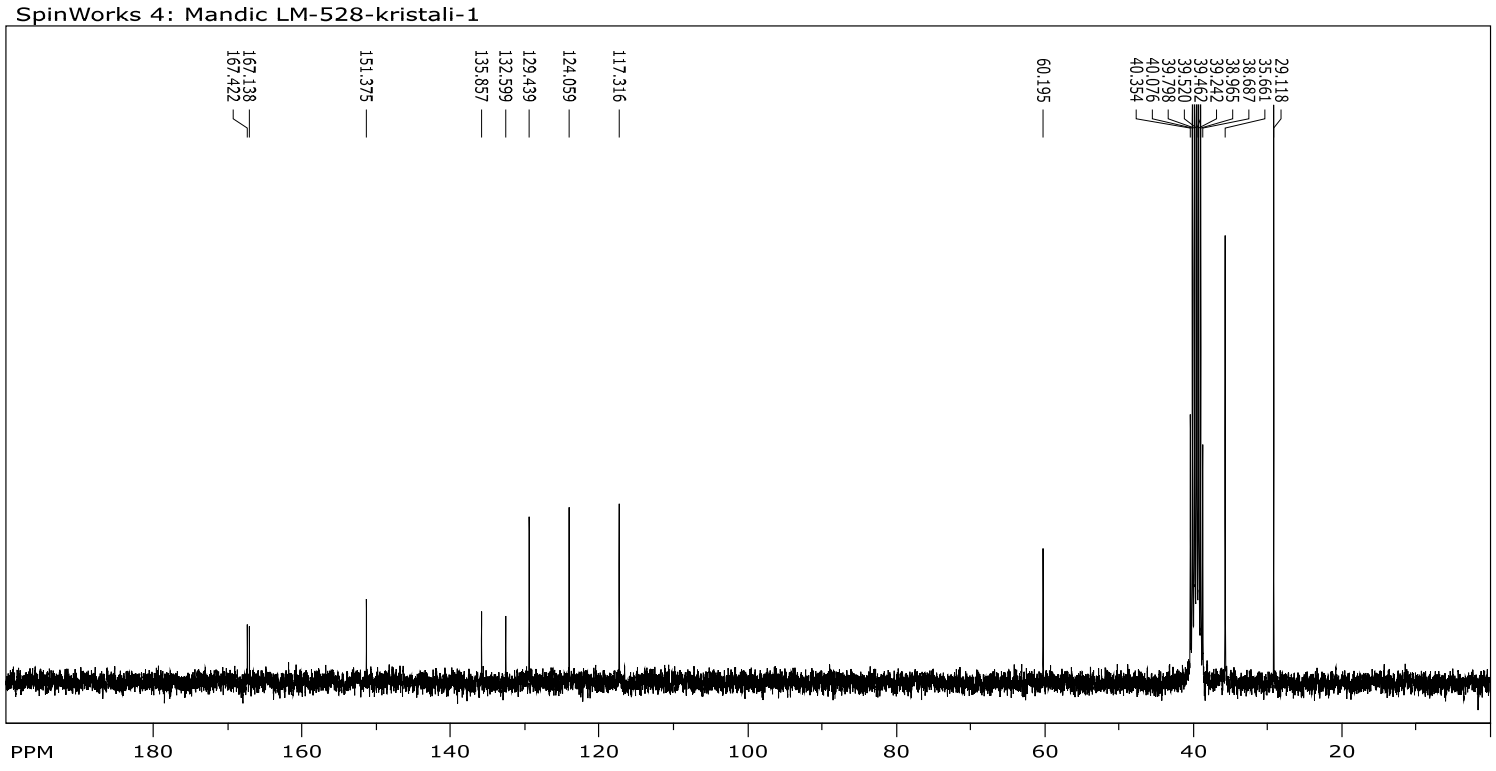

Fig S66. ^{1}H (DMSO-d_6, 600 MHz) NMR spectrum of **6H**.

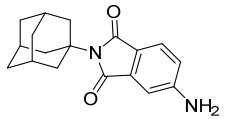

6H

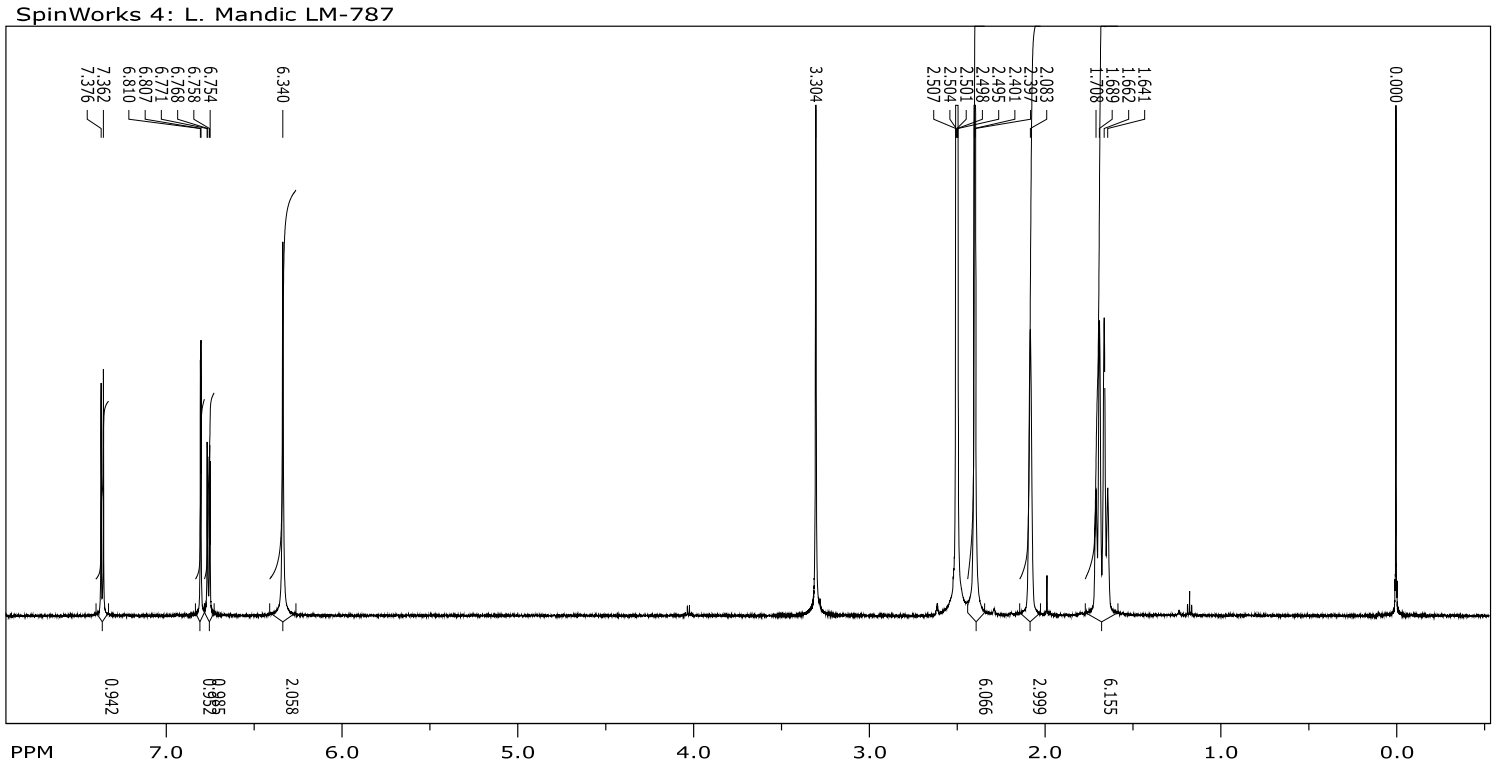

file: K:\NMR (AntiVir)\Compound 3\1H\fid expt: <zg30>
transmitter freq.: 600.135401 MHz
time domain size: 32768 points
width: 12019.23 Hz = 20.0275 ppm = 0.366798 Hz/pt
number of scans: 64

freq. of 0 ppm: 600.130000 MHz
processed size: 32768 complex points
LB: 0.000 GF: 0.0000

Fig S67. ^{13}C (DMSO-d_6, 75 MHz, COM) NMR spectrum of **6H**.

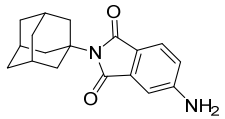

6H

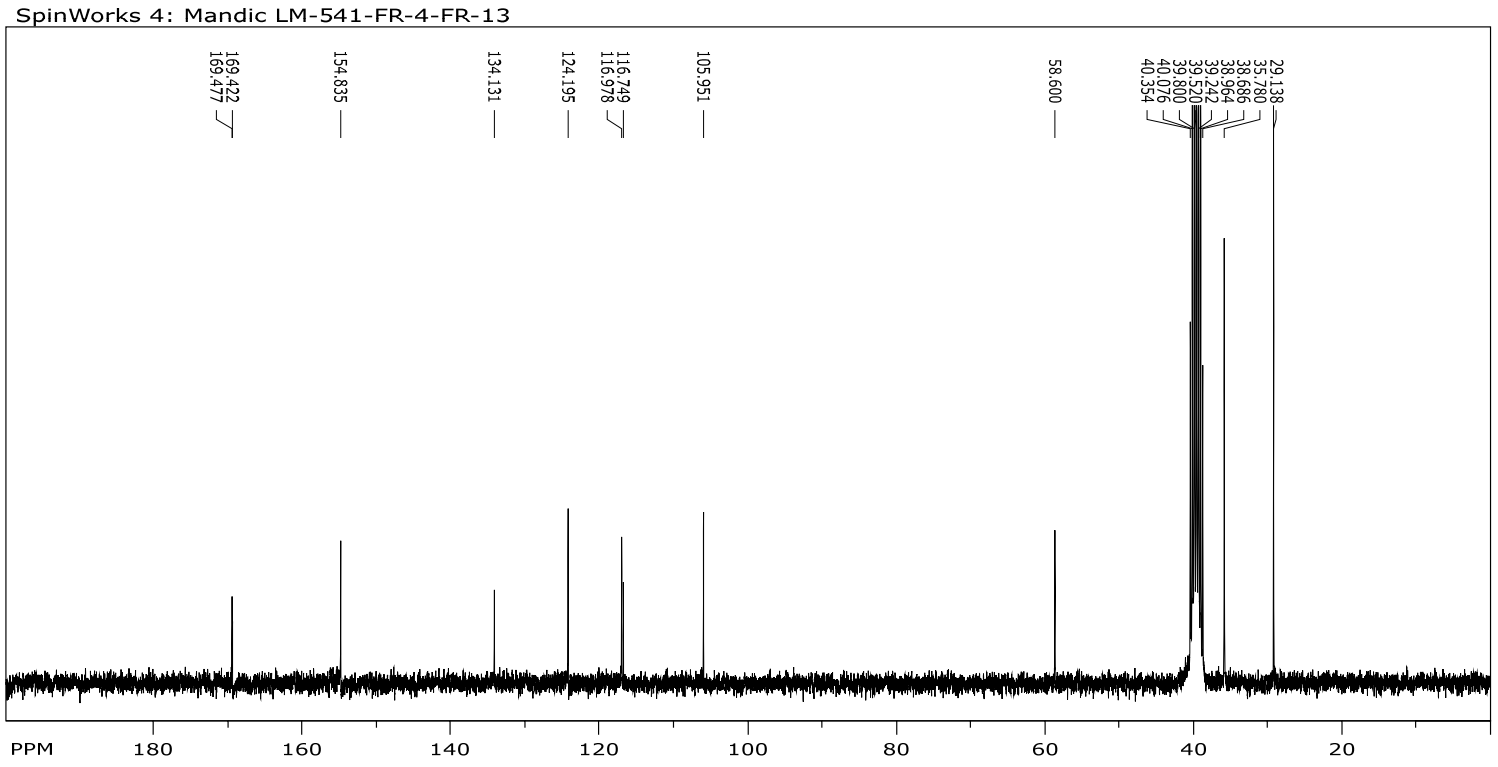

Fig S68. ^{1}H ($CDCl_3$, 600 MHz) NMR spectrum of **3COCH$_3$**.

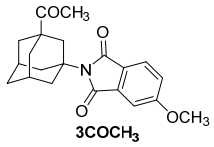

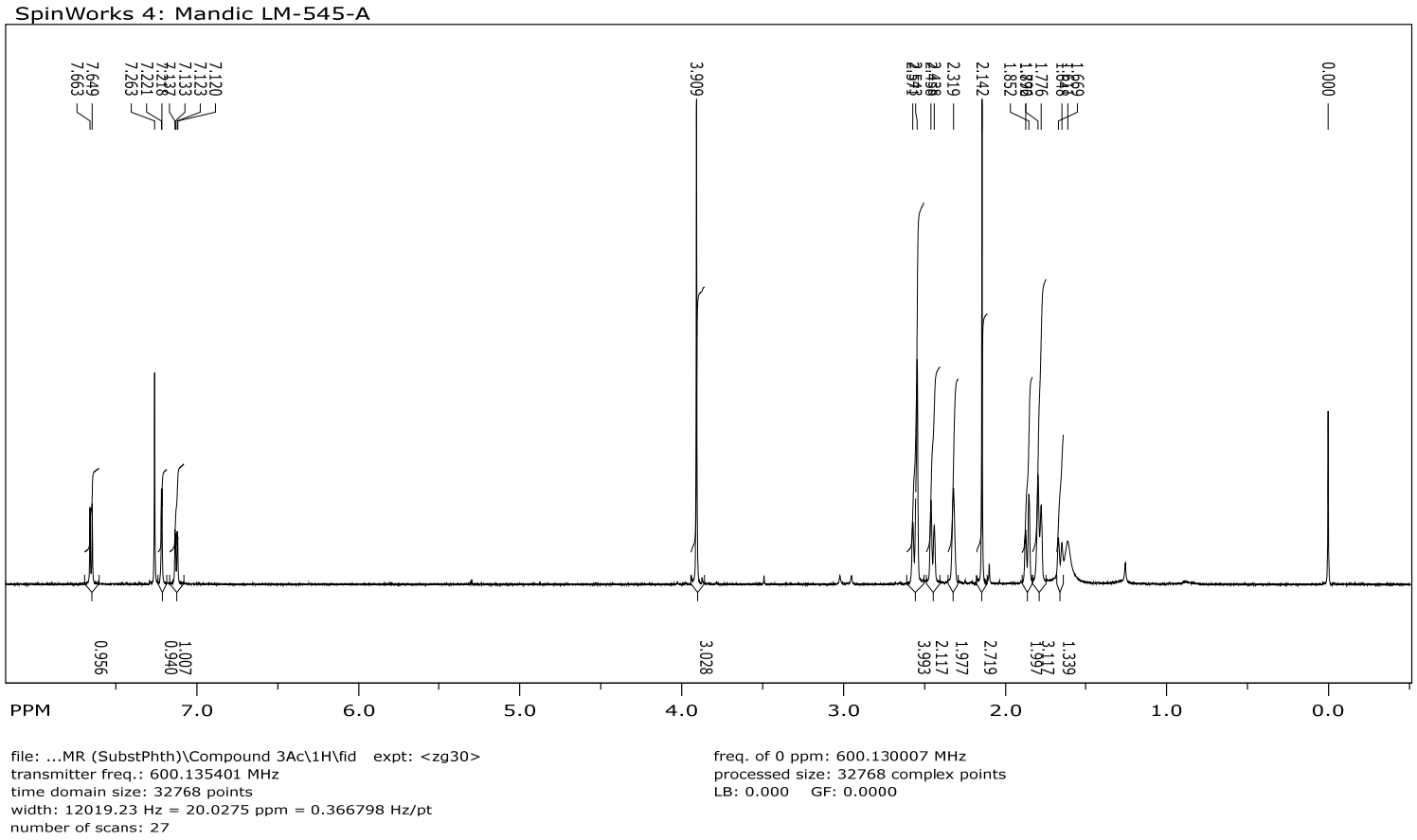

Fig S69. ^{13}C ($CDCl_3$, 150 MHz, COM) NMR spectrum of **3COCH$_3$**.

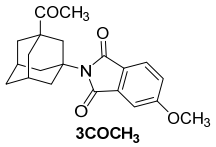

3COCH$_3$

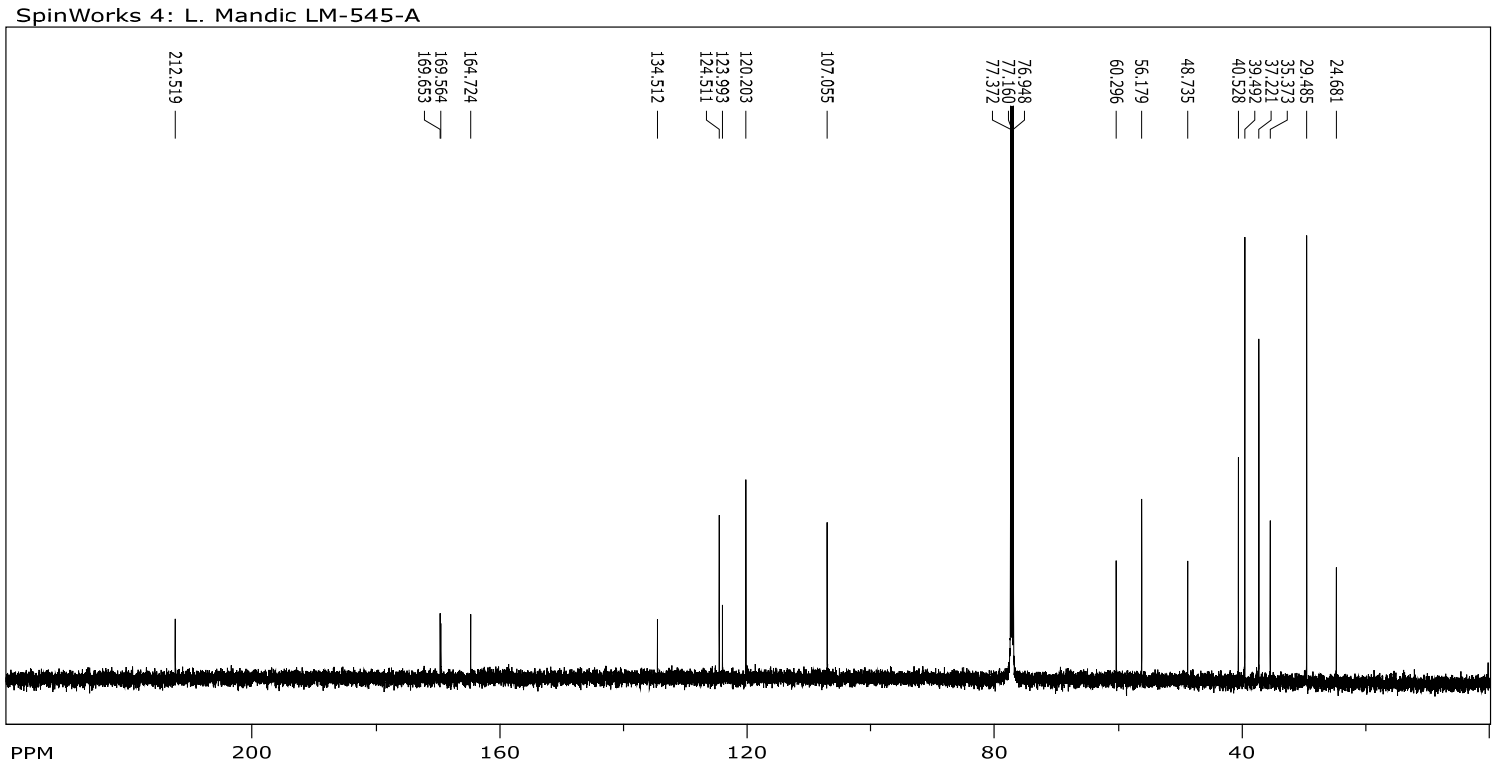

file: ...\3-(4'-OMe)Phth-1-acetylAd\COM\fid expt: <zgpg30>
transmitter freq.: 150.920917 MHz
time domain size: 65536 points
width: 39370.08 Hz = 260.8656 ppm = 0.600740 Hz/pt
number of scans: 1216

freq. of 0 ppm: 150.902787 MHz
processed size: 32768 complex points
LB: 1.000 GF: 0.0000

Fig S70. ^{1}H ($CDCl_3$, 600 MHz) NMR spectrum of **3OH**.

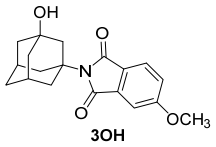

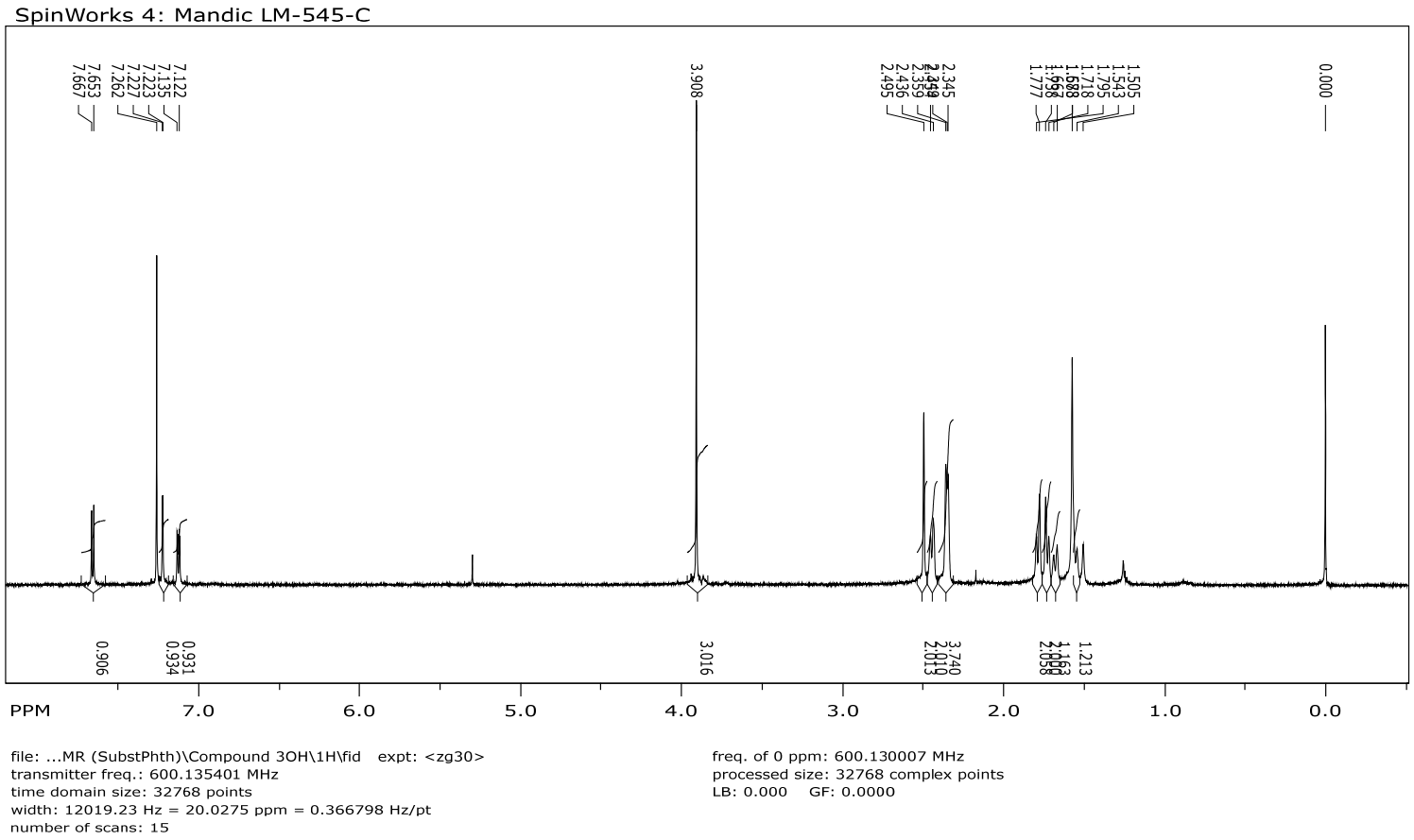

Fig S71. ^{13}C ($CDCl_3$, 150 MHz, COM) NMR spectrum of **3OH**.

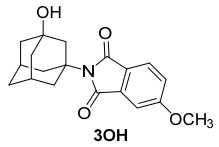

3OH

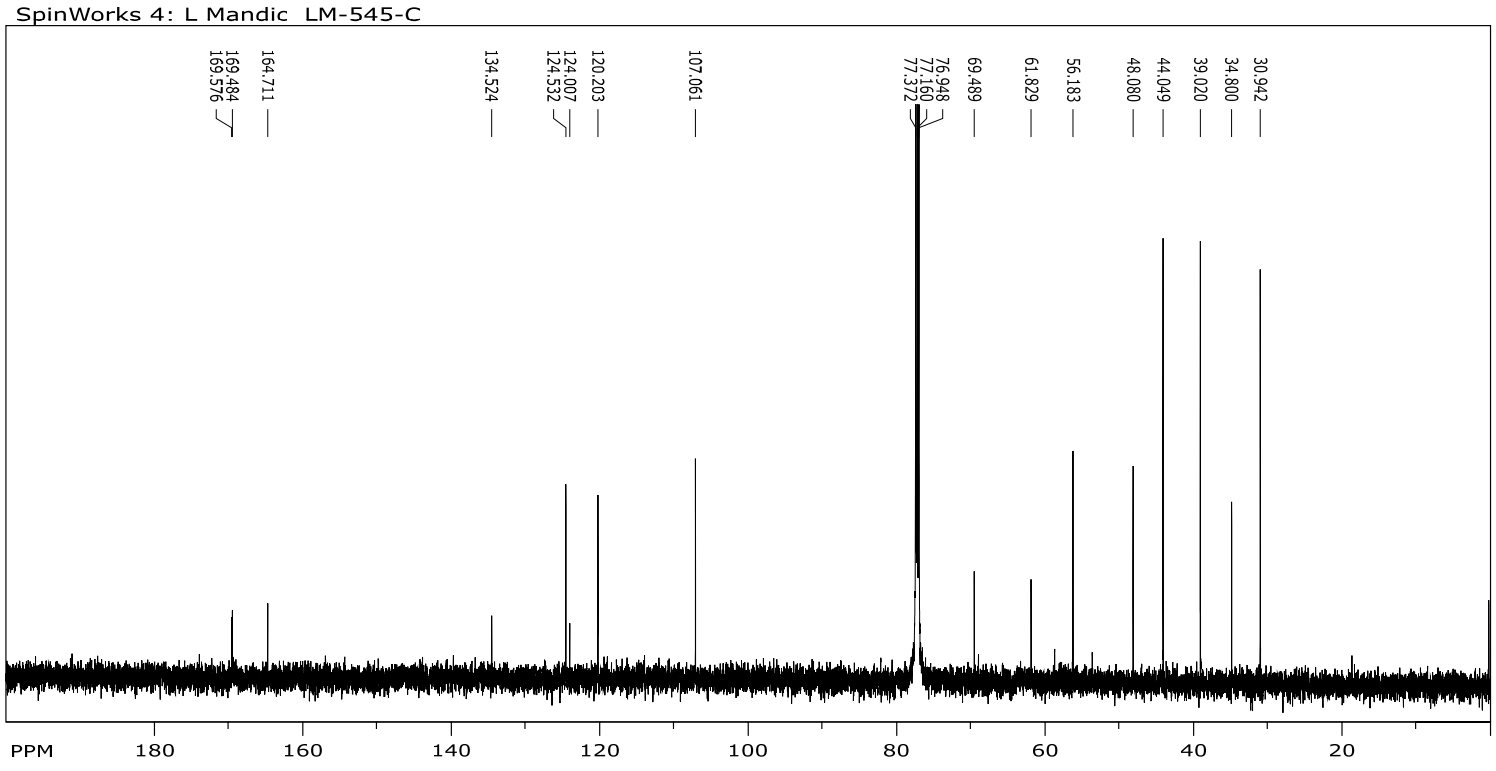

file: ...ives\3-(4'-OMe)PhthAd-1-OH\COM\fid expt: <zgpg30>
transmitter freq.: 150.917899 MHz
time domain size: 32768 points
width: 35971.22 Hz = 238.3496 ppm = 1.097755 Hz/pt
number of scans: 2673

freq. of 0 ppm: 150.902787 MHz
processed size: 32768 complex points
LB: 1.000 GF: 0.0000

Fig S72. ^{1}H (CD_3OD, 300 MHz) NMR spectrum of **4COCH$_3$**.

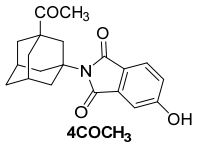

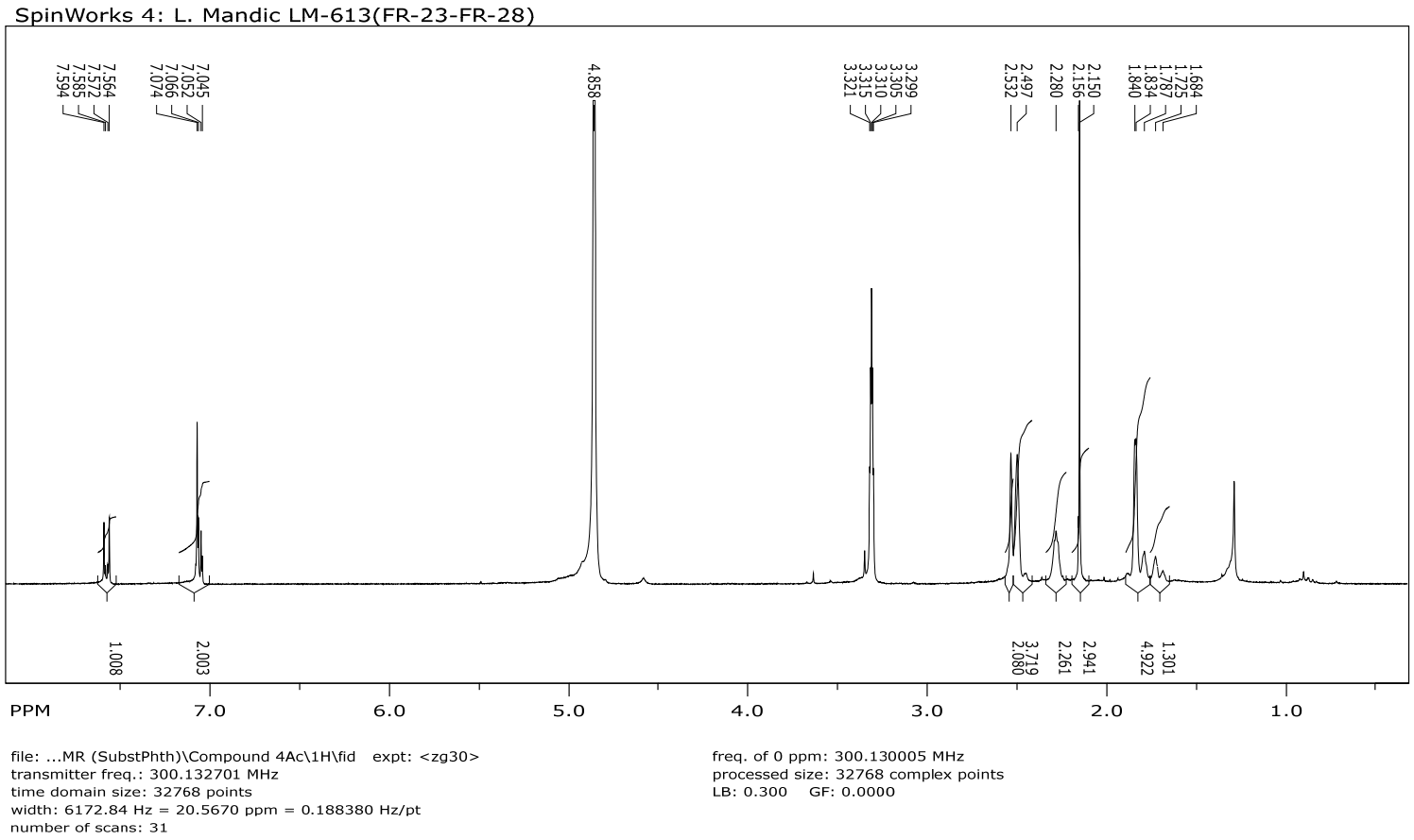

Fig S73. ^{13}C (CD_3OD, 75 MHz, COM) NMR spectrum of **4COCH$_3$**.

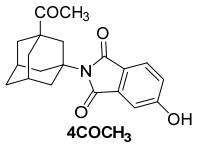

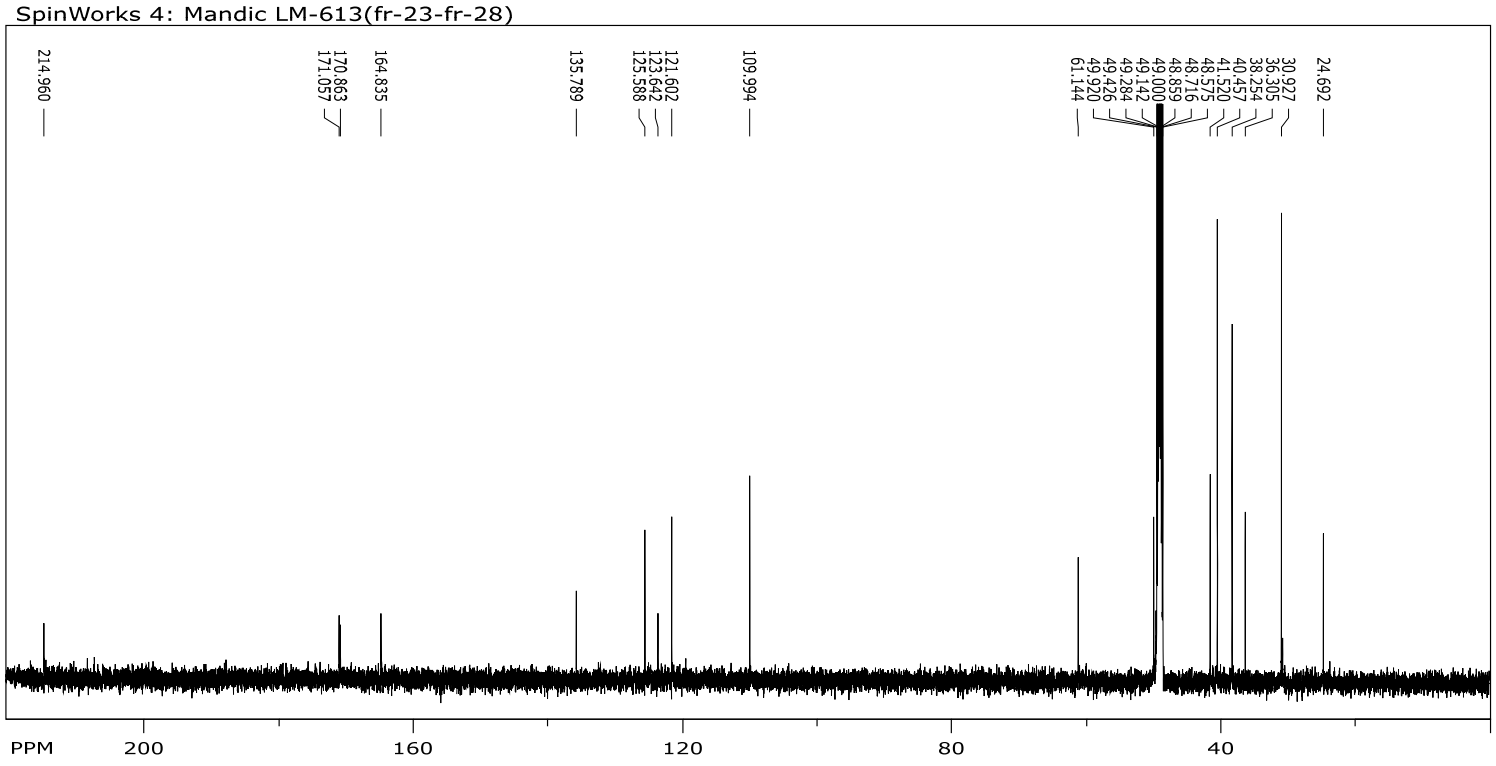

file: ...s\3-(4'-OH)Phth-1-acetylAd\COM\fid expt: <zgpg30>
transmitter freq.: 150.917899 MHz
time domain size: 65536 points
width: 35971.22 Hz = 238.3496 ppm = 0.548877 Hz/pt
number of scans: 4088

freq. of 0 ppm: 150.902594 MHz
processed size: 32768 complex points
LB: 1.000 GF: 0.0000

Fig S74. ^{1}H (CD_3OD, 600 MHz) NMR spectrum of **4OH**.

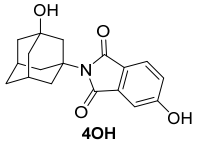

4OH

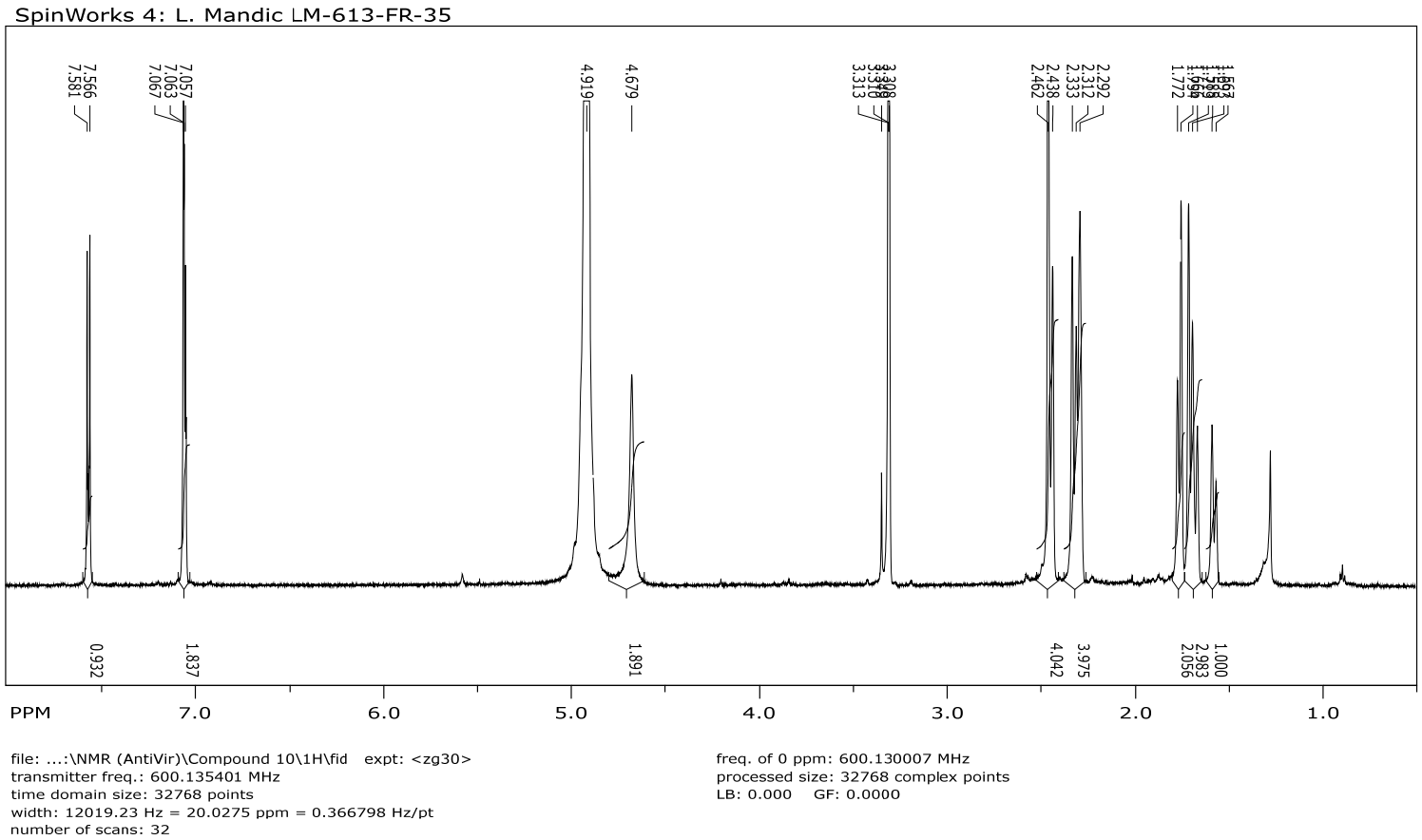

file: ...:\NMR (AntiVir)\Compound 10\1H\fid expt: <zg30>
transmitter freq.: 600.135401 MHz
time domain size: 32768 points
width: 12019.23 Hz = 20.0275 ppm = 0.366798 Hz/pt
number of scans: 32

freq. of 0 ppm: 600.130007 MHz
processed size: 32768 complex points
LB: 0.000 GF: 0.0000

Fig S75. ^{13}C (CD_3OD, 150 MHz, COM) NMR spectrum of **4OH**.

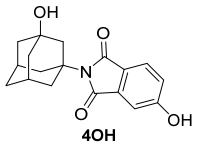

4OH

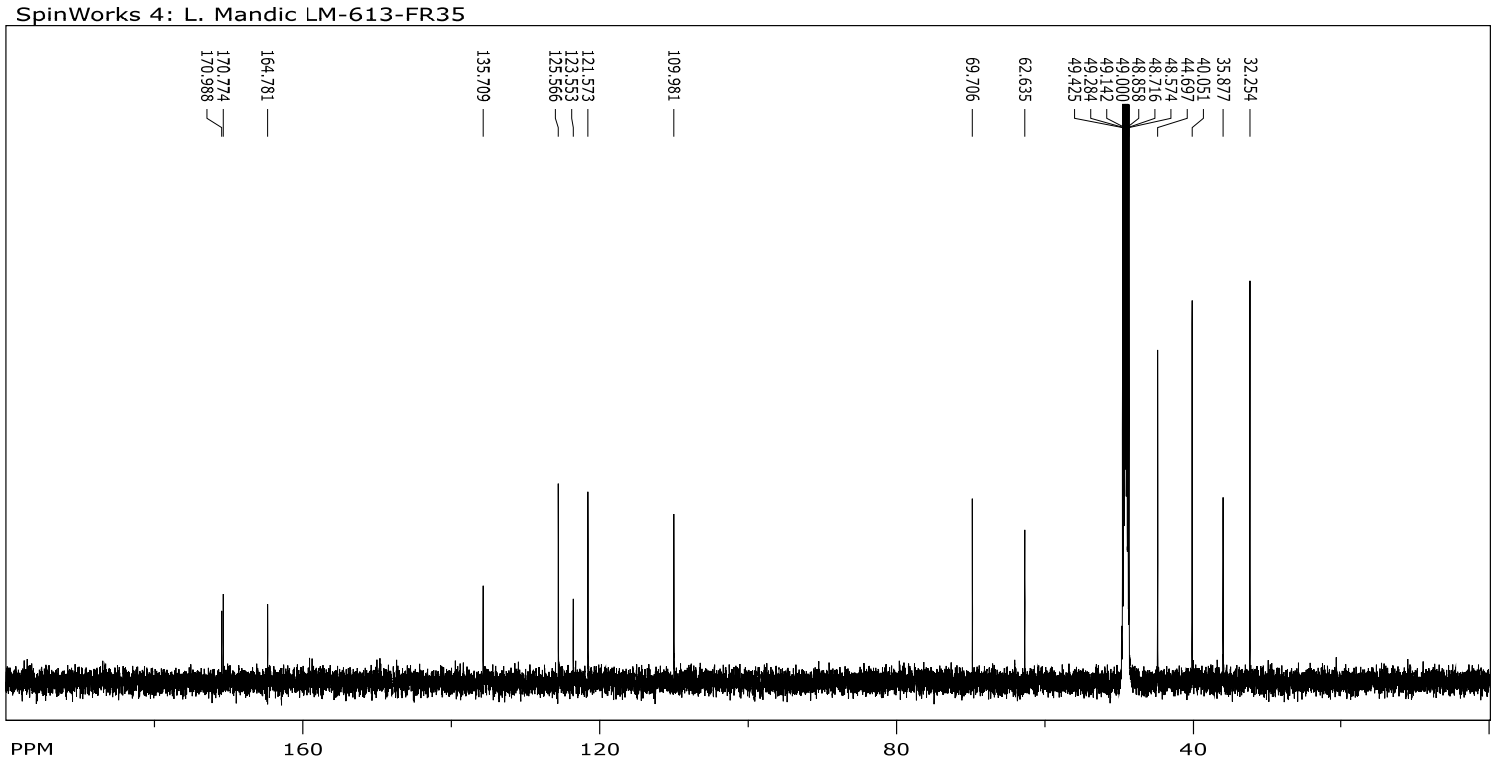

Fig S76. ^{1}H (CD_3OD, 300 MHz) NMR spectrum of **4OOH**.

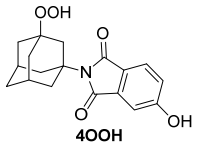

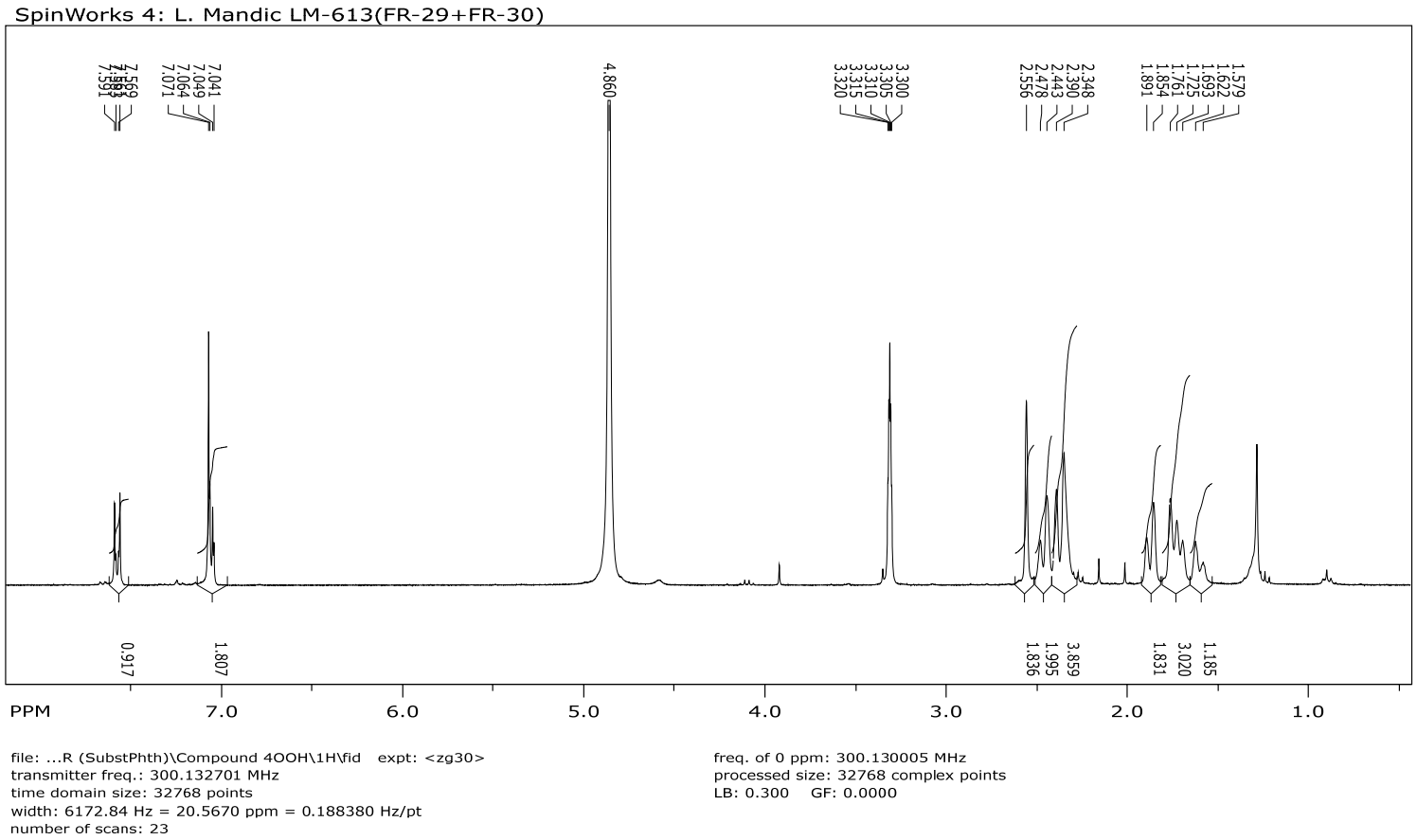

Fig S77. ^{13}C (CD_3OD, 150 MHz, COM) NMR spectrum of **4OOH**.

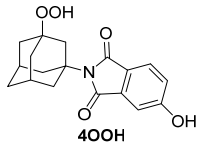

4OOH

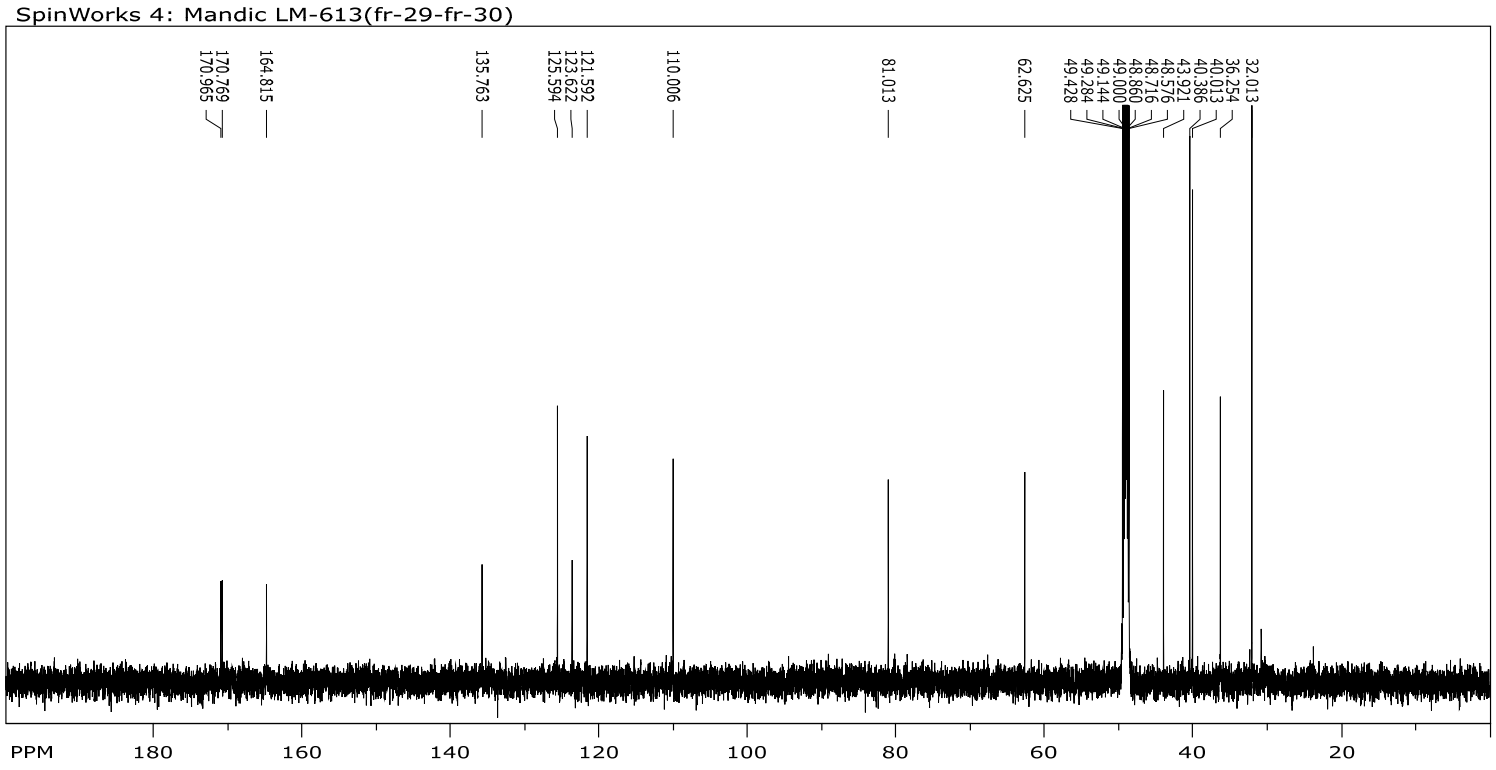

file: ...ives\3-(4'-OH)PhthAd-1-OOH\COM\fid expt: <zgpg30>
transmitter freq.: 150.917899 MHz
time domain size: 65536 points
width: 35971.22 Hz = 238.3496 ppm = 0.548877 Hz/pt
number of scans: 975

freq. of 0 ppm: 150.902595 MHz
processed size: 32768 complex points
LB: 1.000 GF: 0.0000

Fig S78. ^{1}H ($CDCl_3$, 300 MHz) NMR spectrum of **5OH**.

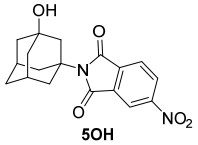

5OH

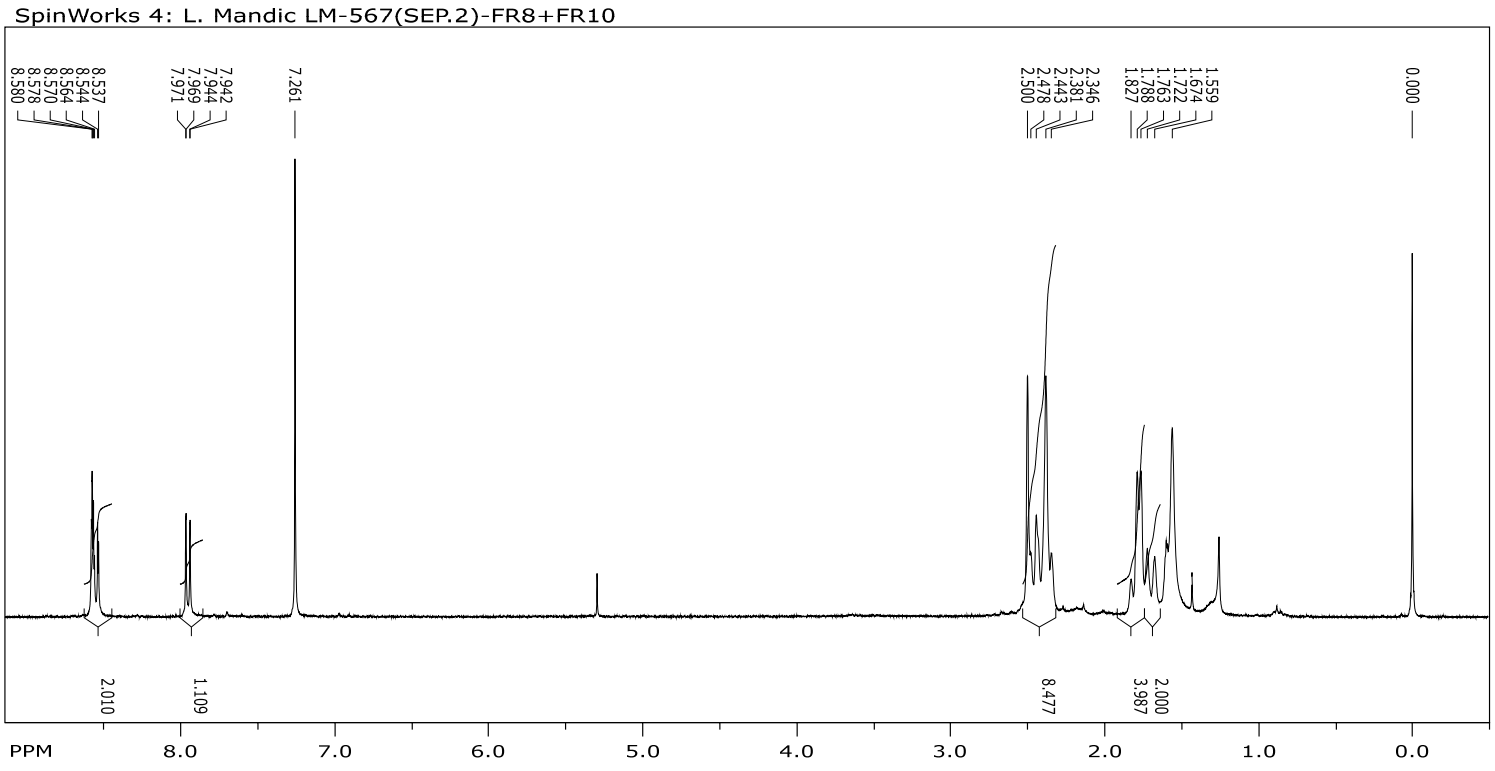

file: ...MR (SubstPhth)\Compound 5OH\1H\fid expt: <zg30>
transmitter freq.: 300.132701 MHz
time domain size: 32768 points
width: 6172.84 Hz = 20.5670 ppm = 0.188380 Hz/pt
number of scans: 25

freq. of 0 ppm: 300.130006 MHz
processed size: 32768 complex points
LB: 0.300 GF: 0.0000

Fig S79. ^{13}C ($CDCl_3$, 75 MHz, COM) NMR spectrum of **5OH**.

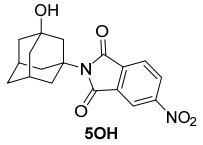

5OH

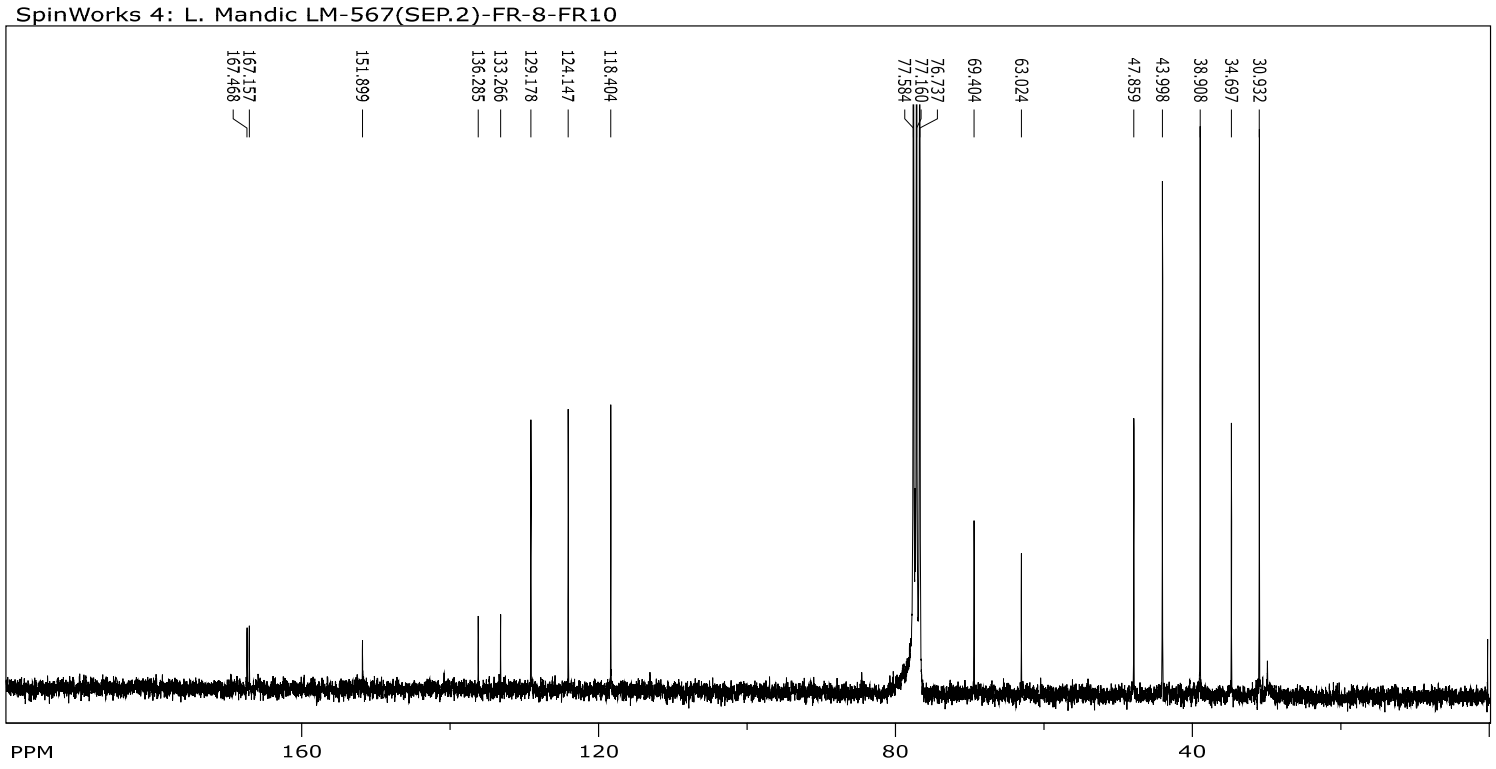

file: ...es\3-(4'-nitro)PhthAd-1-OH\COM\fid expt: <zgpg30>
transmitter freq.: 75.475295 MHz
time domain size: 32768 points
width: 17985.61 Hz = 238.2980 ppm = 0.548877 Hz/pt
number of scans: 30065

freq. of 0 ppm: 75.467737 MHz
processed size: 32768 complex points
LB: 1.000 GF: 0.0000

Fig S80. ^{1}H ($CDCl_3$, 300 MHz) NMR spectrum of **5OOH**.

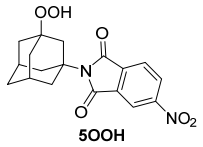

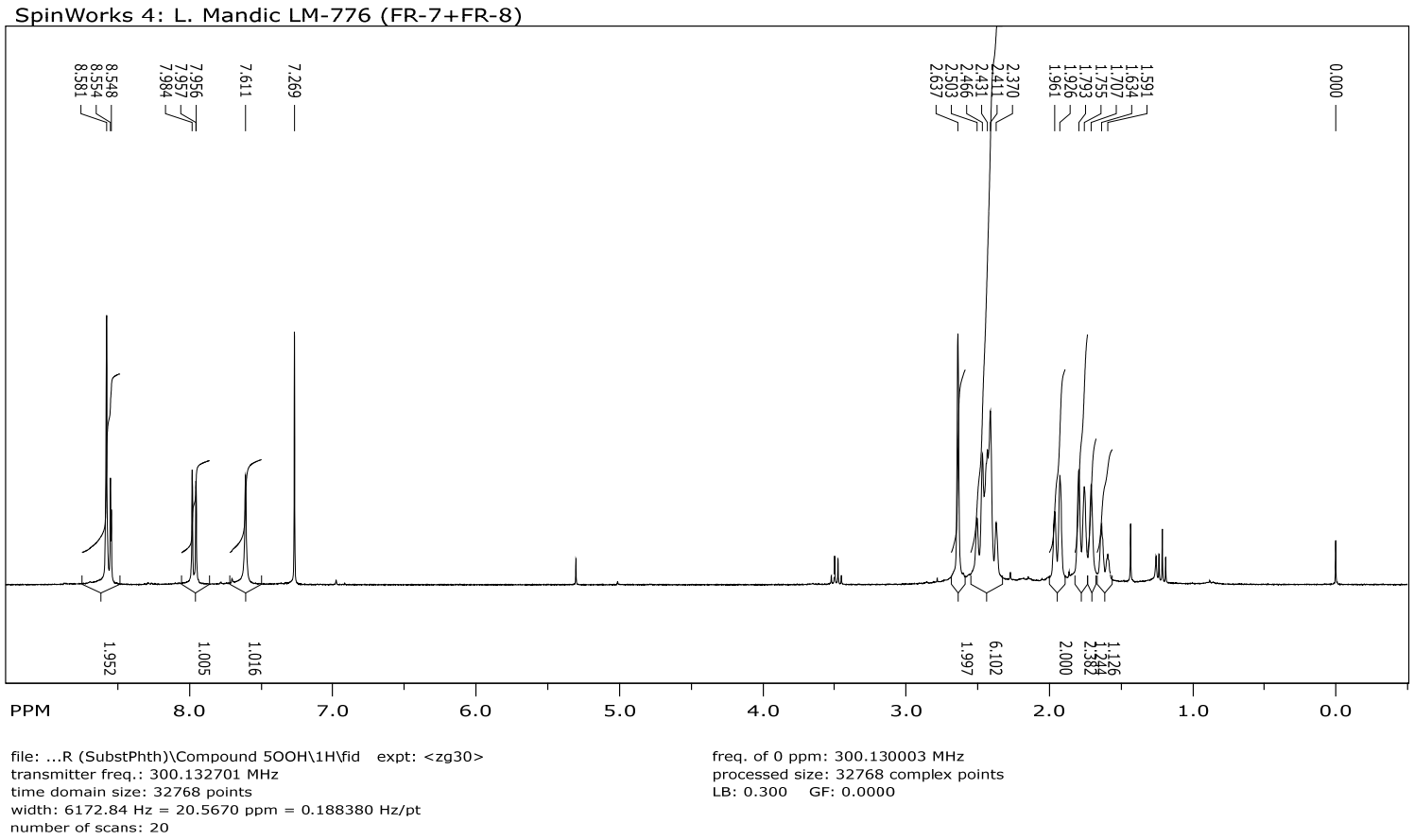

Fig S81. ^{13}C ($CDCl_3$, 75 MHz, COM) NMR spectrum of **5OOH**.

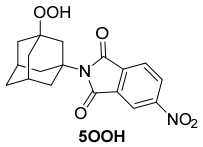

5OOH

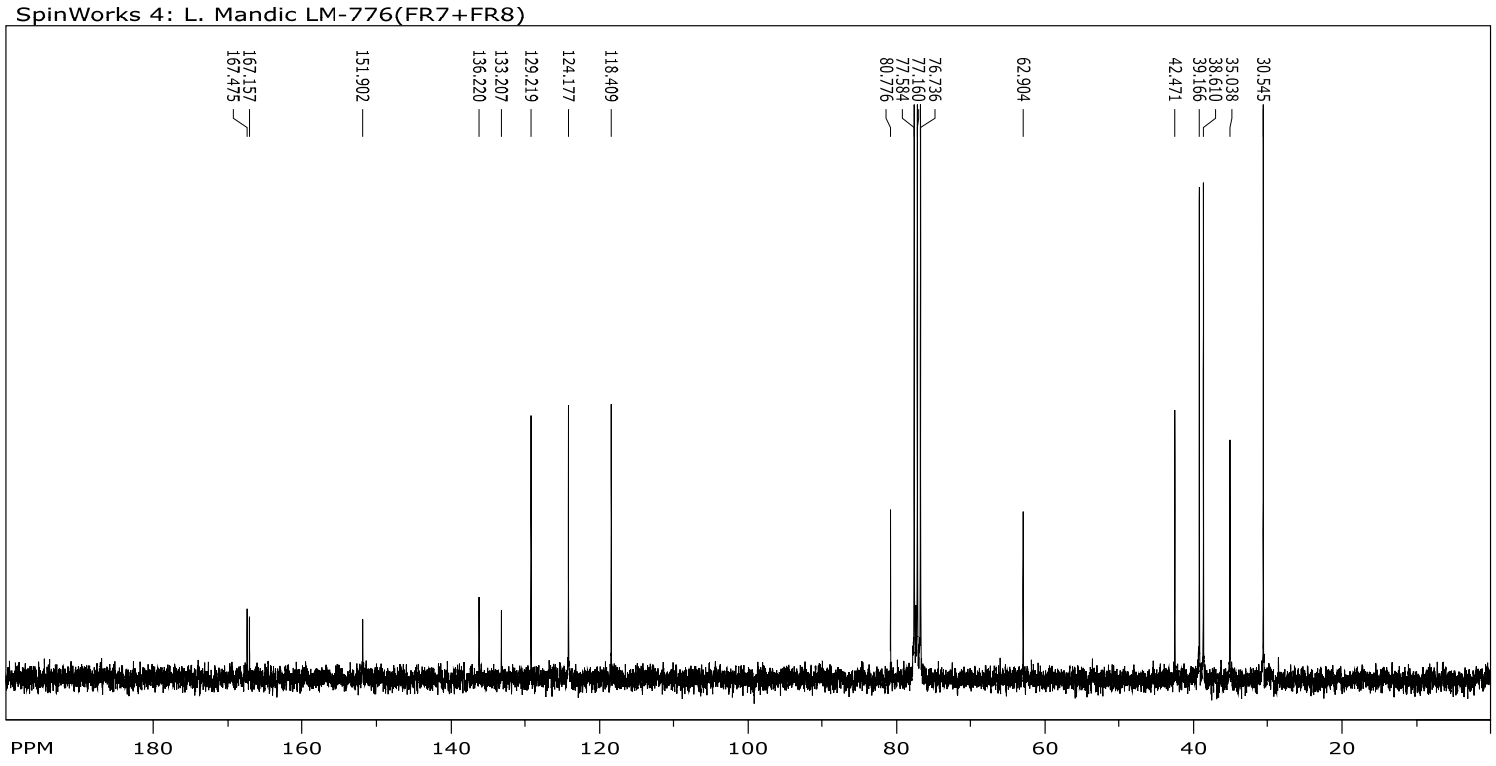

file: ...s\3-(4'-nitro)PhthAd-1-OOH\COM\fid expt: <zgpg30>
transmitter freq.: 75.475295 MHz
time domain size: 32768 points
width: 17985.61 Hz = 238.2980 ppm = 0.548877 Hz/pt
number of scans: 557

freq. of 0 ppm: 75.467738 MHz
processed size: 32768 complex points
LB: 1.000 GF: 0.0000